

**Observation of Isoprene Hydroxynitrates in the Southeastern
United States and Implications for the Fate of NO_x**

F. Xiong¹, K. M. McAvey¹, K. A. Pratt^{1,3}, C. J. Groff¹, M. A. Hostetler¹, M. A. Lipton¹, T. K. Starn⁴, J. V. Seeley⁵, S. B. Bertman⁶, A. P. Teng⁷, J. D. Crounse⁸, T. B. Nguyen⁸, P. O. Wennberg^{7,8}, P. K. Misztal⁹, A. H. Goldstein^{9,10}, A. B. Guenther¹¹, A. R. Koss^{12,13}, K. F. Olson⁹, J. A. de Gouw^{12,13}, K. Baumann¹⁴, E. S. Edgerton¹⁴, P. A. Feiner¹⁵, L. Zhang¹⁵, D. O. Miller¹⁵, W. H. Brune¹⁵ and P. B. Shepson^{1,2}

[1] Department of Chemistry, Purdue University, West Lafayette, IN

[2] Department of Earth, Atmospheric and Planetary Sciences, Purdue University, West Lafayette, IN

[3] Department of Chemistry, University of Michigan, Ann Arbor, MI

[4] Department of Chemistry, West Chester University of Pennsylvania, West Chester, PA

[5] Department of Chemistry, Oakland University, Rochester, MI

[6] Department of Chemistry, Western Michigan University, Kalamazoo, MI

[7] Division of Engineering and Applied Science, California Institute of Technology, Pasadena, CA

[8] Division of Geophysical and Planetary Sciences, California Institute of Technology, Pasadena, CA

[9] Department of Environmental Science, Policy, & Management, University of California at Berkeley, Berkeley, CA

[10] Department of Civil and Environmental Engineering, University of California at Berkeley, Berkeley, CA

[11] Atmospheric Sciences and Global Change Division, Pacific Northwest National Laboratory, Richland, WA

[12] Cooperative Institute for Research in Environmental Sciences, Boulder, CO

[13] NOAA Earth System Research Laboratory, Boulder, CO

[14] Atmospheric Research & Analysis, Inc., Cary, NC

[15] Department of Meteorology, Pennsylvania State University, University Park, PA

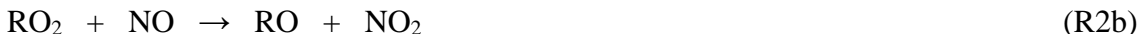
Correspondence to: P. B. Shepson (pshepson@purdue.edu)

Abstract

Isoprene hydroxynitrates (IN) are tracers of the photochemical oxidation of isoprene in high NO_x environments. Production and loss of IN have a significant influence on the NO_x cycle and tropospheric O₃ chemistry. To better understand IN chemistry, a series of photochemical reaction chamber experiments was conducted to determine the IN yield from isoprene photooxidation at high NO concentrations (>100 ppt). By combining experimental data and calculated isomer distributions, a total IN yield of 9(+4/-3)% was derived. The result was applied in a zero-dimensional model to simulate production and loss of ambient IN observed in a temperate forest atmosphere, during the Southern Oxidant and Aerosol Study (SOAS) field campaign, from May 27 to July 11, 2013. The 9% yield was consistent with the observed IN/(MVK+MACR) ratios observed during SOAS. By comparing field observations with model simulations, we identified NO as the limiting factor for ambient IN production during SOAS, but vertical mixing at dawn might also contribute (~27%) to IN dynamics. A close examination of isoprene's oxidation products indicates that its oxidation transitioned from a high-NO dominant chemical regime in the morning into a low-NO dominant regime in the afternoon. A significant amount of IN produced in the morning high NO regime could be oxidized in the low NO regime, and a possible reaction scheme was proposed.

1 Introduction

Isoprene (C_5H_8) accounts for approximately half of the global non-methane biogenic volatile organic compound (BVOC) emissions (Guenther et al., 2006) and has a significant influence on the budgets of OH, O_3 and NO_x (Horowitz et al., 2007). Isoprene oxidation by OH in the presence of NO_x can lead to the formation of isoprene hydroxynitrates (IN), as described in Reactions (R1) and (R2). The chain-terminating Reaction (R2a) removes peroxy radicals (RO_2) and NO from the atmosphere and decreases tropospheric O_3 production (Carter and Atkinson, 1996). IN serves as a temporary NO_x reservoir, and the transport and photo-oxidative decomposition of these compounds can further modulate NO_x and O_3 concentrations (Horowitz et al., 2007; Paulot et al., 2012; Xie et al., 2013). Gas-phase organic nitrates can also partition into the particle phase and undergo hydrolysis, contributing to the growth of secondary organic aerosols (SOA) (Jacobs et al., 2014; Rindelaub et al., 2015).



The initial OH addition (followed by O_2) to isoprene (Reaction R1) produces eight isomeric RO_2 radicals. Reaction of these RO_2 radicals with NO proceeds primarily via two reaction pathways (Reaction R2a and b). Laboratory studies suggest that the nitrate formation channel (Reaction R2a) is minor compared to the alkoxy radical (RO) formation channel (Reaction R2b), with reported total IN yields ranging from 4% to 14% (Chen et al., 1998; Patchen et al., 2007; Lockwood et al., 2010; Paulot et al., 2009; Sprengnether et al., 2002; Tuazon and Atkinson, 1990). Reaction (R2a) leads to the formation of eight IN isomers, including four β -IN isomers and four δ -IN isomers (Table 1). The wide range of reported IN yields has led to uncertainty in quantifying isoprene's influence on the NO_x cycle and O_3 enhancement (Xie et al., 2013; Horowitz et al., 2007; Paulot et al., 2012). Isoprene hydroxynitrates can also be produced at night through NO_3 -initiated isoprene oxidation with a yield around 20%, adding to a total organic nitrate yield of 65-70% (Rollins et al., 2009; Perring et al., 2009; Kwan et al., 2012). The major daytime IN sink is reaction with OH, which leads to a lifetime of 2.5 to 6.5 hours,

83 according to a recent kinetics study (Lee et al., 2014b). At night, IN is more susceptible
84 to loss from ozonolysis, and potentially NO₃ oxidation when the NO_x concentration is
85 high (Xie et al., 2013). IN have been observed in the ambient environment, primarily in
86 forested areas under the influence of anthropogenic NO_x plumes (Grossenbacher et al.,
87 2001; Giacomelli et al., 2005; Grossenbacher et al., 2004; Beaver et al., 2012; Lee et al.,
88 2014a). During the BEARPEX 2009 study conducted in the Sierra Nevada Mountains of
89 California, IN constituted 38% of the total organic nitrates (Beaver et al., 2012).

90 Methods to quantify organic nitrates include infrared spectroscopy (IR), thermal
91 dissociation-laser induced fluorescence (TD-LIF) spectroscopy, chemiluminescence, gas
92 chromatography (GC)-based separation and detection techniques, and mass spectrometry
93 (MS) (Rollins et al., 2010; Tuazon and Atkinson, 1990; Sprengnether et al., 2002; Day et
94 al., 2002; O'Brien et al., 1995; Beaver et al., 2012; Lee et al., 2014a; Lockwood et al.,
95 2010; Paulot et al., 2009; Giacomelli et al., 2005; Grossenbacher et al., 2004; Patchen et
96 al., 2007; Hartsell et al., 1994; Kwan et al., 2012; Teng et al., 2015). IR, TD-LIF, and
97 chemiluminescence can only measure total organic nitrates because they respond solely
98 to the nitrooxy functional group (Day et al., 2002; Rollins et al., 2010; Tuazon and
99 Atkinson, 1990; Sprengnether et al., 2002; O'Brien et al., 1995; Hartsell et al., 1994).
100 GC- and MS-based methods can speciate organic nitrates and have been employed
101 previously to quantify IN in both laboratory and field studies (Lockwood et al., 2010;
102 Patchen et al., 2007; Giacomelli et al., 2005; Paulot et al., 2009; Lee et al., 2014a;
103 Grossenbacher et al., 2004; Beaver et al., 2012; Kwan et al., 2012). For MS-based
104 techniques, the fragile O-NO₂ bond in organic nitrates often fragments during ionization
105 (Perring et al., 2009), so soft-ionization methods with reagent ion such as H⁺(H₂O)₄,
106 CF₃O⁺, and I⁺ are necessary to detect the molecular ion for organic nitrates (Patchen et al.,
107 2007; Beaver et al., 2012; Lee et al., 2014a; Crounse et al., 2006).

108 Here we present a comprehensive laboratory and field study of the formation of IN from
109 isoprene reaction with OH. In the summer of 2013, we quantified ambient IN in rural
110 Alabama for 6 weeks during the Southern Oxidant and Aerosol Studies (SOAS,
111 <http://soas2013.rutgers.edu/>). In parallel with the field study, laboratory experiments were
112 conducted to determine the yield of IN from isoprene oxidation. For laboratory
113 experiments, we synthesized authentic standards for the quantification of IN, using

multiple calibration techniques. The IN yield obtained from lab experiments was applied in a zero-dimensional model to simulate IN production and loss in the atmosphere, which was then compared with the measurements from SOAS, to examine our understanding of atmospheric IN chemistry.

2 Experiment

2.1 CIMS IN calibration

A chemical ionization mass spectrometer (CIMS) was used to measure IN concentrations during the chamber experiments and the SOAS field study. The instrument is similar to the one described by Liao et al. (2011), which uses $I(H_2O)_n^-$ to form iodide clusters with the analyte compounds.

Two authentic standards, 4,3-IN and 1,4-IN (a mixture of *trans*- and *cis*-1,4-IN), were synthesized to determine the sensitivity of CIMS toward IN isomers. 1,4-IN was prepared using the nitrification method described by Lee et al. (2014b), and the sample was used after flash column chromatography without further purification to separate the *trans* and *cis* isomers. 4,3-IN was prepared by nitrification of (1-methylethenyl)oxirane, and the epoxide was synthesized following Harwood et al. (1990).

The IN gas-phase sample for CIMS calibration was prepared by evaporating an IN/C₂Cl₄ standard solution of known volume into 50 L of clean air. The IN concentration in the standard solution was determined with NMR and FTIR, and the results from the two methods were consistent within 15%. Multiple CIMS calibrations for 4,3-IN were performed, and the results did not deviate more than 15% after 1.5 years (Supplement Sect. 1). The average sensitivity of 4,3-IN normalized to the reagent ion signal was $2.3(\pm 0.3) \times 10^{-3} \text{ ppt}^{-1}$.

The 1,4-IN calibration was conducted following the same procedures. Since the 1,4-IN standard contained a mixture of *trans*- and *cis*-1,4-IN, the measured sensitivity was a weighted average of both isomers. The relative abundance of the *trans*- and *cis*-1,4-IN isomers was obtained from NMR, and their individual sensitivities were estimated using a least-squares method (Supplement Sect. 2). The CIMS sensitivity was $3(\pm 2) \times 10^{-4} \text{ ppt}^{-1}$ for *trans*-1,4-IN and $1.3(\pm 0.3) \times 10^{-3} \text{ ppt}^{-1}$ for *cis*-4,1-IN.

As we were unable to synthesize the 1,2-IN standard in the condensed phase, a relative method was used, where the CIMS was interfaced with a GC equipped with an electron capture detector (ECD, Figure 1) to determine the CIMS sensitivity of 1,2-IN relative to 4,3-IN. A mixture of the eight IN isomers was generated by irradiation of a mixture of isoprene, isopropyl nitrite, and NO. The IN mixture was cryo-focused at the head of a 4 m Rtx-1701 column that separated the IN isomers, and the effluent was split into two fused-silica deactivated transfer columns, directed simultaneously to the CIMS and the ECD.

As the CIMS was operated with water addition to the sample gas before ionization, the GC-ECD/CIMS setup enabled direct observation of the influence of water vapor to the sensitivity of the two dominant IN isomers. Figure 2 shows the GC-ECD/CIMS chromatograms with and without water added to the CIMS. The change in retention time was the result of change in initial oven temperature setting, which had little influence on the elution temperature of IN. 1,2-IN and 4,3-IN were the dominant IN isomers and 1,2-IN eluted before 4,3-IN, according to a recent study using the same stationary phase (Nguyen et al., 2014b). 1,2-IN and 4,3-IN are expected to have the same ECD sensitivity, because the ECD has similar response to all mono-nitrates and the hydroxyl group in hydroxynitrate has no influence on ECD sensitivity (Hao et al., 1994). Therefore, the CIMS sensitivity of 1,2-IN relative to 4,3-IN was calculated as the ratio of the CIMS signal intensity to the corresponding ECD signal intensity, for the pair of isomers. The calculated relative CIMS sensitivity was $0.37(\pm 0.06)$ with water and $0.95(\pm 0.06)$ without water added, determined as the average of three trials for each setup. The result indicated that water addition to the sample air lowered the CIMS sensitivity to the 1,2-IN isomer. The small abundance of the other isomers makes it difficult to obtain reliable quantification through this method. Therefore, the sensitivities for cis- and trans-1,4-IN were obtained with a synthesized standard.

The CIMS sensitivities toward alkyl alcohols and alkyl nitrates are both around 5 orders of magnitude smaller than its sensitivity toward the isoprene hydroxynitrates. Hence, it is the combination of the OH group and the NO₃ group, as well as their relative positions that has the dominant influence on the CIMS sensitivity, which will affect how the molecule binds with the iodide ion, while the structure of the carbon backbone would

have little effect. For the IN isomers, the relative positions of the OH group and the nitrate group are α,β position, $\text{trans-}\alpha,\delta$ position and $\text{cis-}\alpha,\delta$ position. We assume the same sensitivity can be applied to isomers within each structural group, namely β -isomers, *trans- δ* isomers and *cis- δ* isomers. This assumption is consistent with our observation of identical sensitivity for 1,2-IN and 4,3-IN isomers when water is not added to the CIMS. For the case with water addition to CIMS, the smaller sensitivity of the 1,2-IN was caused by the smaller amount of 1,2-IN available for detection, as 1,2-IN is lost inside the instrument, rather than from a fundamental difference in the ionization efficiency of 1,2-IN. Primary nitrates (δ -IN, 3,4-IN, and 2,1-IN) and secondary nitrates (4,3-IN) are not as likely to be affected by water (Hu et al., 2011). As a result, *cis*-1,4-IN was used as a surrogate for *cis*-4,1-IN, and *trans*-1,4-IN was used as a surrogate for *trans*-4,1-IN. For the β -IN isomers, 1,2-IN had to be considered separately due to its loss inside the instrument, but 4,3-IN was used as a surrogate for 3,4- and 2,1-IN isomers. Our assignment of CIMS sensitivities for IN isomers is consistent with reports from Lee et al. (2014a). Given the significant difference in sensitivity for different IN isomers, the CIMS IN data have to be interpreted with the knowledge of relative IN isomer distribution, which depends on both IN production and loss. Since the IN isomer distribution was not measured in either the laboratory or the field studies, model simulation was used to estimate the relative abundance of IN isomers. The distribution of IN isomers during the chamber experiments was estimated using an iterative method (Supplement Sect. 3.1). For IN measurement during SOAS, a diurnal average of the changing IN isomer distribution (Figure S9) was estimated and applied to calibrate IN data for each individual day. The isomer-weighted IN sensitivity changed by less than 20% throughout the day (Supplement Sect. 3.2).

2.2 Isoprene chamber experiments

Seven experiments were conducted in the 5500 L Purdue photochemical reaction chamber (Chen et al., 1998) to determine the yield of IN from OH-initiated isoprene oxidation in the presence of NO_x . OH was generated from the photolysis of isopropyl nitrite. The starting conditions for the experiments are listed in Table 2. Each experiment

was initiated by switching on the UV lamps and was considered complete when half of the isoprene was consumed or the NO concentration dropped to around 5 ppb.

The IN concentration was measured continuously during each experiment with the CIMS. Chamber air was sampled through a 5.2 m long inlet, made of 0.8 cm ID heated (constant 50 °C) FEP Teflon tubing. A total flow of 5 liters per minute (lpm) was pulled through the inlet into a custom-built three-way valve system (Liao et al., 2011), where 2 lpm was sub-sampled into the CIMS through a 0.51 mm orifice. Water vapor was added downstream of the orifice to humidify the sample air to reduce the influence that variations in ambient RH and temperature have on the distribution of $I(H_2O)_n^-$ clusters. Laboratory tests showed that with constant H₂O addition, the CIMS sensitivity is not dependent on ambient air humidity (Supplement Sect. 6). The fractional loss inside the 50 °C sampling inlet was measured to be 5 % for a mixture of the eight IN isomers.

Isoprene and its oxidation products, methyl vinyl ketone (MVK) and methacrolein (MACR), were quantified with a proton-transfer reaction linear ion trap mass spectrometer (PTR-LIT MS), with measurement precision of 3 ppb and accuracy of $\pm 17\%$ (Mielke et al., 2010). MVK and MACR were observed as the same nominal mass without further differentiation for relative isomeric abundance. The NO concentration was measured through chemiluminescence using the total reactive nitrogen instrument (TRENI) (Lockwood et al., 2010), and the addition of isopropyl nitrite did not cause any interference signal for TRENI during the chamber experiments.

One wall loss experiment was conducted by keeping the IN isomers produced from isoprene oxidation in the dark chamber and sampling the chamber air with CIMS periodically for four hours. No significant IN loss was observed, so no wall loss correction was applied for IN measurement.

2.3 CIMS SOAS measurement

During SOAS, the CIMS was used to measure ambient IN concentrations continuously from May 26st to July 11th, 2013 at the Centerville (CTR) site (32.90° N, 87.25° W). The CTR site is located about 50 miles south of Birmingham and Tuscaloosa near the Talladega National Forest, a region abundant with pine and oak trees. The CIMS was

operated under the same conditions as those during the chamber experiments, in terms of voltage setting, gas flow and sample humidification. Air was sampled from 5.3 m above the ground, with the same inlet (heated to constant 50 °C) and valve system that were used for chamber experiments. The CIMS three-way valve system was used to allow automated background measurement and in-situ Br₂ calibration to monitor instrument stability. The background was determined by passing ambient air through nylon wool coated with sodium bicarbonate for 2 minutes every 15 minutes (Crounse et al., 2006). Laboratory tests suggested that the scrubber removes isoprene-derived organic nitrates, including hydroxynitrates, carbonyl nitrates and hydroxyperoxy nitrates, and acids such as nitric acid and formic acid. Br₂ calibration was performed hourly by adding a 30 sccm Br₂/N₂ flow from a Br₂ permeation device to the ambient air being sampled into the CIMS for 2 min. The CIMS sensitivity to IN was calibrated relative to the Br₂ sensitivity, which were both normalized to the reagent ion signal I(H₂¹⁸O)⁺. The Br₂ output rate from the permeation device was determined daily with the optical absorption method following Liao et al. (2011). The averaged Br₂ output of the permeation source throughout the campaign was 60(±8) ng/min, which was 1.8(±0.2) ppb when diluted with ambient air.

2.4 0D Model for IN Data Interpretation

A zero-dimensional (0D) model based on the Master Chemical Mechanism (MCMv3.2) (Jenkin et al., 1997; Saunders et al., 2003) was used to investigate the production and loss of IN in the chamber and in the SOAS field study. The mechanism was updated for recent experimental and theoretical studies of isoprene chemistry, including the interconversion of isomeric isoprene RO₂ radicals (LIM1) (Peeters et al., 2014), IN reaction rate constants for OH and O₃ (Lee et al., 2014b), IEPOX reaction rate constants for OH (Bates et al., 2014) and the branching ratio for NO₃ addition to isoprene (Fan and Zhang, 2004).

For the IN observations during SOAS, our analysis is focused on the production and loss of IN. Therefore, the 0D model for the SOAS data analysis was constrained to the observed concentrations of the major species involved in the IN chemistry, including isoprene, HO_x, O₃, NO_x, α-pinene, β-pinene and limonene. The NO₂ photolysis frequency in the 0D model (*J*_{NO2}) was calculated using the Tropospheric Ultraviolet & Visible

(TUV) Radiation Model (Madronich and Flocke, 1998) for clear sky conditions with 300 DU ozone, and the model input was scaled relative to observed radiation. The photolysis frequencies for all the other species were scaled relative to J_{NO_2} at zero-degree solar zenith angle.

Because the 0D model does not take into account the changes in IN concentration as IN was transported to and out of the measurement site both vertically and horizontally, the ratio of total IN concentration to the sum of methyl vinyl ketone (MVK) and methacrolein (MACR) was used to compare the model results with observations. Major sources of MVK and MACR include isoprene ozonolysis (Grosjean et al., 1993) and OH-initiated isoprene oxidation (Liu et al., 2013). Because IN, MVK and MACR are produced simultaneously in the isoprene photochemical oxidation process, the ratio $[\text{IN}]/([\text{MVK}]+[\text{MACR}])$ may reduce the influence of dilution caused by vertical mixing and changing boundary layer height, making results from the 0D model comparable to ambient observations. Besides chemical loss to reaction with OH, O_3 and NO_3 , the model also included loss for dry deposition for IN, MVK and MACR, with averaged daytime deposition velocities of 1.5cm/s, 0.7cm/s and 0.4cm/s (Nguyen et al., 2015; Zhang et al., 2002).

Isoprene data from the PTR-ToF-MS measurement (Misztal et al., In preparation) were used to constrain the model and its MVK+MACR data were used for model-observation comparison for most days. The MVK and MACR data from the GC-MS measurement (Gilman et al., 2010) were used when knowledge of the relative abundance of MVK and MACR was required to calculate their initial concentrations in the model and when PTR-ToF-MS data were unavailable. The PTR-ToF-MS data were used primarily because of its higher time resolution. Model constraints on α -pinene, β -pinene and limonene concentrations were based on measurements from GC-MS, and 2D-GC when GC-MS data were unavailable.

3 Results

3.1 IN yield from chamber experiments

The IN yield was calculated from the production of IN relative to the loss of isoprene, using data obtained in the photochemical reaction chamber experiments. The isomer-weighted IN sensitivity is expected to change during each experiment, as IN isomers are lost to OH consumption with different reaction rate constants. To account for the change in IN isomer distribution during each experiment, an iterative method was applied to derive a self-consistent set of total IN yield, IN isomeric distribution and isomer-weighted IN sensitivity (Supplement 3.1). IN loss by OH oxidation was corrected (Atkinson et al., 1982) with an isomer-weighted rate constant to account for the difference in OH reactivity for different isomers (Lee et al., 2014b). The correction factor was around 25% by the end of each experiment. Figure 3 shows the results from the IN yield chamber experiments. The average IN yield was 9%, based on the slope of Δ IN vs. $(-\Delta$ isoprene). We note that the yield has no apparent [NO] dependence with [NO] varying in the range from 125 ppb to 2400 ppb.

The relative uncertainty for isoprene concentrations is 17% based on instrument calibration. The uncertainty for IN concentrations is caused by both the uncertainty in the CIMS sensitivity for each IN isomer and the uncertainty in the relative abundance of the IN isomers. Through a sensitivity test on the RO₂ interconversion rate constants of the LIM1 mechanism (Supplement Sect. 5), the IN measurement uncertainty was estimated to be +23%/-20%. The fractional loss for the CIMS inlet was 4(±6)%, making the IN measurement uncertainty to be +24%/-20%. The uncertainty in the reported rate constants for IN oxidation could cause 20 % error when IN data was corrected for OH consumption. Therefore, the overall relative uncertainty in our IN yield is +36%/-33% and we report our total IN yield to be 9(+4/-3)% to encompass all the measurement uncertainties. This result lies in the middle of the 4-14% range of IN yields determined from previous experiments (Chen et al., 1998; Patchen et al., 2007; Lockwood et al., 2010; Paulot et al., 2009; Sprengnether et al., 2002; Tuazon and Atkinson, 1990). Previous IN studies conducted in our group using GC methods consistently resulted in lower IN yields (Chen et al., 1998; Lockwood et al., 2010). We partially attribute the discrepancy of our

previous and current work to the possible loss of the 1,2-IN isomer in the GC column and metal sample injection system. This work employed MS to quantify IN during the chamber experiments to circumvent these problems. The current yield result will be applied in the 0D model to simulate IN concentrations during SOAS. The model-measurement agreement offers a metric to evaluate the validity of the laboratory-derived IN yield

3.2 Observation of IN during SOAS

Figure 4 shows the temporal profile of total IN mixing ratio observed during the SOAS field study with an averaging 10-minute time resolution. In general, fast IN production was observed after sunrise. On average, the concentration rose to peak around 70 ppt at 10:00 AM (Figure 5) and then decreased to a minimum around 10 ppt by 6:00 AM the next day, as a result of vertical mixing, boundary layer expansion, dry deposition and further oxidation. IN concentrations were significantly lower from Jul 4 to Jul 8, due to wet deposition and less photochemical reactivity caused by continuous rain events.

In contrast to the IN average diurnal profile (Figure 5), the diurnal profiles for isoprene, OH, and NO_x and MVK+MACR, each peaked at different times of the day (Figure 6). While IN and MVK + MACR are products of the parallel RO₂ + NO Reactions (R2a and b), the diurnal MVK + MACR concentrations are more consistent with the temporal profiles of isoprene, OH and O₃ with peak concentration around 1:00 PM when radiation was strong. The decrease in IN, and continued increase of MVK and MACR around 10:00 AM can be attributed to the competition among the four RO₂ loss channels (R2, R3, R4, and R5).



The fraction of RO₂ loss to NO reaction is defined as γ , which is calculated with the following equation.

$$\gamma = \frac{k_{\text{RO}_2+\text{NO}}[\text{NO}]}{k_{\text{RO}_2+\text{NO}}[\text{NO}] + k_{\text{RO}_2+\text{HO}_2}[\text{HO}_2] + k_{\text{RO}_2+\text{RO}_2}[\text{RO}_2] + k_{\text{isomerize}}} \quad (1)$$

Isoprene RO₂ loss to permutation reactions R4 was calculated assuming [RO₂]=[HO₂], and the rate constant $1.6 \times 10^{-13} \text{ cm}^3 \text{ molecule}^{-1} \text{ s}^{-1}$ was used (Jenkin et al., 1997). Isoprene RO₂ loss rates for reaction with NO and HO₂ (R2 and R3) were calculated based on observed NO and HO₂ concentrations, using rate constants $k_{\text{RO}_2+\text{NO}} = 9 \times 10^{-12} \text{ cm}^3 \text{ molecule}^{-1} \text{ s}^{-1}$ and $k_{\text{RO}_2+\text{HO}_2} = 1.61 \times 10^{-11} \text{ cm}^3 \text{ molecule}^{-1} \text{ s}^{-1}$ (Saunders et al., 2003; Stevens et al., 1999). The sum of the first-order RO₂ loss rate for reaction with NO, HO₂ and RO₂ was 0.01-0.07 s⁻¹ (Figure 7a). Therefore, contribution from 1,5-H shift for β-RO₂ was negligible, due to the small isomerization rate constant (Peeters et al., 2014). However, for isoprene *cis*-δ-RO₂, the 1,6-H shift rate constant is on the order of 0.1-1 s⁻¹ (Peeters et al., 2009; Crounse et al., 2011; Peeters et al., 2014). This fast isomerization depletes *cis*-δ-RO₂ radicals rapidly to form closed-shell products, e.g. hydroperoxy aldehyde (HPALD), and makes the relative abundance of *cis*-δ-RO₂ radicals very small (~1%, Supplement Sect. 4). For this reason, $k_{\text{isomerize}}$ was omitted from the calculation of γ, but the yield of total RO₂ was incorporated when estimating the production rate of total IN, to account for rapid loss of *cis*-δ-RO₂ to 1,6-H shift. In addition, the fast 1,6-H isomerization for *cis*-δ-RO₂ decreased the production rates of δ-IN among the IN isomers. With this smaller production rates and their faster loss rates to OH and O₃ (Lee et al., 2014b), the relative abundance of δ-IN during this field study was much smaller than what have been observed in laboratory studies (Lockwood et al., 2010; Paulot et al., 2009).

The calculated diurnal average of the γ value is shown in Figure 7b. For RO₂ radicals that were lost to reaction with NO or HO₂, the RO₂+NO reaction was the sole contributor in the early morning, but it was surpassed by RO₂+HO₂ reaction before noon, as the NO concentration decreased steadily throughout the day. The IN production rate was calculated with the following equation.

$$P_{\text{IN}} = k_{\text{ISOP}+\text{OH}}[\text{OH}][\text{ISOP}] \cdot \Phi \cdot \gamma \cdot \alpha \quad (2)$$

α is the branching ratio ($=k_{2a}/(k_{2a} + k_{2b})$) for isoprene RO₂ + NO reaction for nitrate formation. Φ is the yield of total RO₂ from OH addition to isoprene that are available to react with NO, HO₂ and RO₂, with an RO₂ lifetime in the range of 10~20s. The calculated Φ is 0.83 (Supplement Sect. 4), with contribution from β-RO₂ being 0.81, *cis*-

376 δ -RO₂ being 0.01 and *trans*- δ -RO₂ being 0.02, and the remaining 17% products from
 377 isoprene OH oxidation are closed-shell species such as HPALD.

378 The γ value peaked around 6:00 AM to 8:00 AM when the isoprene and OH
 379 concentrations were relatively low. During this period, the IN production rate was limited
 380 by the availability of RO₂. In the afternoon, when isoprene RO₂ was more abundant with
 381 higher isoprene and OH concentrations, the IN production rate was limited by the
 382 availability of NO, and decreased with the declining γ value (Fig. 7b). The declining γ
 383 value could lead IN loss from OH oxidation to exceed IN production, making IN peak
 384 around the time when HO₂ reaction became the major RO₂ loss channel ($\gamma < 0.5$). In this
 385 relatively clean environment, MVK and MACR production continued through isoprene
 386 ozonolysis (Grosjean et al., 1993) and OH oxidation in the low NO regime (Liu et al.,
 387 2013). The MVK+MACR production rate was calculated using the following equation.

$$\begin{aligned}
 388 \quad P_{\text{MVK+MACR}} &= k_{\text{ISOP+OH}}[\text{OH}][\text{ISOP}] \cdot \Phi_{\beta} \cdot \gamma \cdot (1-\alpha) \\
 389 &+ k_{\text{ISOP+OH}}[\text{OH}][\text{ISOP}] \cdot \Phi \cdot (1-\gamma) \cdot 0.06 \\
 390 &+ k_{\text{ISOP+O}_3}[\text{O}_3][\text{ISOP}] \cdot 0.61 \qquad (3)
 \end{aligned}$$

391 Φ_{β} denotes the yield of isoprene β -RO₂, the precursors for MVK+MACR, and the
 392 calculated Φ_{β} was 0.81 (Supplement Sect. 4). The term $k_{\text{ISOP+OH}}[\text{OH}][\text{ISOP}] \cdot \Phi_{\beta} \cdot \gamma \cdot (1-\alpha)$ is
 393 the production rate of MVK+MACR with the isoprene β -RO₂ undergoing the RO₂+NO
 394 reaction pathway. The term $k_{\text{ISOP+OH}}[\text{OH}][\text{ISOP}] \cdot \Phi \cdot (1-\gamma) \cdot 0.06$ is the production rate of
 395 MVK+MACR when the isoprene RO₂ proceeds via HO₂+RO₂ reaction pathways to form
 396 MVK+MACR with an overall yield of 6% (Liu et al., 2013). The term
 397 $k_{\text{ISOP+O}_3}[\text{O}_3][\text{ISOP}] \cdot 0.61$ is the production rate of MVK+MACR from isoprene
 398 ozonolysis, with a total yield of 61% (Grosjean et al., 1993).

399 As shown in Figure 7b, the production rates of IN and MVK+MACR both plateaued
 400 around 10:00 AM. For MVK+MACR, the decrease was later compensated with
 401 production from the HO₂ and O₃ pathway, and the production rate peaked around 2:00
 402 PM when radiation was strong. For IN, however, its production rate did not increase with
 403 radiation due the limited availability of NO (small γ value). Therefore, the change in the
 404 relative importance of the two RO₂ sinks, RO₂+NO and RO₂+HO₂, is likely one of the

reasons that the IN concentration peaked earlier than the MVK+MACR concentration during SOAS.

The early morning increase in IN concentration could imply significant contribution from downward mixing of accumulated IN in the residual layer (RL), as the inversion is broken up after dawn (Hastie et al., 1993). When the earth surface cools in the evening, the remnants of the upper daytime boundary layer are isolated from the lower region near the ground, and the RL forms. The RL contains the same amount of isoprene, IN, and NO_x as is found near the ground around sunset, thus serving as an IN reservoir at night (Neu et al., 1994). While IN in the nighttime boundary layer (NBL) is slowly lost to dry deposition, IN in the RL, which is isolated from the ground, is better preserved. In addition, IN production from reaction of isoprene with NO_3 may also contribute to RL IN, but this process is not as important in the NBL, because the $\text{NO}_3 + \text{NO}$ reaction decreases the NO_3 concentration near the ground (Stutz, 2004). As a result, the IN concentration in the RL is expected to be higher than that in the NBL before dawn. Perhaps more importantly, the relative volume fraction of NBL vs. RL is small (~ 0.1), and thus surface level nighttime chemistry cannot contribute significantly to the surface IN increase at $\sim 10\text{am}$. During sunrise, IN in the RL can mix downward, which in combination with photochemical IN production leads to an increase in IN near the ground. The relative importance of these two processes will be assessed with our 0D model in the following section.

It is worth mentioning that the nighttime ground-level IN production from $\text{NO}_3 +$ isoprene can afford a different IN isomer distribution, which can influence the isomer-weighted IN sensitivity. However, the 0D model simulation of IN isomer distribution has included IN formation from the $\text{NO}_3 +$ isoprene pathway. Therefore, our interpretation of the SOAS IN measurement data has considered the changing IN isomer distribution from both the OH- and the NO_3 -initiated IN production near ground. The isomeric distribution applied to IN production from $\text{NO}_3 +$ isoprene was 31.1% *trans*-4,1-IN, 12.8% *cis*-4,1-IN, 40.5% 2,1-IN, 0.6% *trans*-1,4-IN, 2.4% *cis*-1,4-IN, 5.5% 3,4-IN, 0.4% 1,2-IN and 0.7% 4,3-IN, based on the theoretical branching ratios proposed by Zhao and Zhang (2008). This isomer composition is consistent with the experimental results of Schwantes et al. (2015) that NO_3 addition to the C1 position of isoprene was dominant, which could

lead to the formation of 42% 2,1-IN and 44-46% 4,1-IN. Since δ -4,1-IN constitutes an important fraction of IN formation from the NO_3 + isoprene reaction, the uncertainty in the relative yield of *trans*-4,1-IN and *cis*-4,1-IN has the largest influence on the isomer-weighted CIMS sensitivity to the IN isomers, as the CIMS sensitivity for *cis*-4,1-IN is over 4 times larger than for the *trans*-4,1-IN. By assuming δ -4,1-IN consists of only the *cis* isomer or the *trans* isomer, we calculated that the isomer-weighted IN sensitivity changed from $1.68 \times 10^{-3} \text{ ppt}^{-1}$ to $1.24 \times 10^{-3} \text{ ppt}^{-1}$, equivalent to a 35% change in calculated IN concentration. This IN sensitivity range is slightly larger than the model-derived IN sensitivity (Figure S10), which is closer to $1.2 \times 10^{-3} \text{ ppt}^{-1}$ at night. Therefore, the nighttime IN concentration may be potentially biased high by up to 35%, but the general trend of the diurnal IN concentrations and the IN concentrations during the daytime should not be affected.

3.3 0D model for IN photochemistry during SOAS

Due to limited availability of overlapping data for model input from multiple instruments, ambient data for the following 12 days were used: Jun 14, Jun 16, Jun 22-Jun 23, Jun 25-Jul 1 and Jul 3. For each day, only the daytime chemistry (5:00 AM - 7:00 PM) was simulated, when photochemical reactivity was high. The observed IN and MVK+MACR concentrations at 5:00 AM were used as the initial concentrations for simulations. For isoprene, α -pinene, β -pinene, limonene, NO, NO_2 , OH, HO_2 , and O_3 , the model concentrations were constrained to observations for the entire modeling period. The branching ratio for IN formation resulting from the isoprene RO_2 + NO reaction was set to 0.09 for all isomers, which is based on our measured 9% yield from the chamber experiments. As mentioned above, to avoid the complication in the simulation of the absolute concentration variability from transport and changing boundary layer height, we compared the simulated and observed $[\text{IN}]/([\text{MVK}]+[\text{MACR}])$ ratio to evaluate the model.

Figure 8a shows the temporal profiles of the modeled and observed $[\text{IN}]/([\text{MVK}]+[\text{MACR}])$ ratio for the selected 12 days. To gain a statistical overview of the model and observation comparison, the 12-day average was calculated (Figure 8b). The 0D model generally agrees with the observed ratio, lending support to the IN

branching ratio determined in the chamber experiments. However, the morning increase was underestimated by the model on certain days (Jun 14, Jun 16, Jun 29, Jul 1 and Jul 3), while on other days (Jun 23 and Jun 25-Jun 27), the decrease rate for the $[IN]/([MVK]+[MACR])$ ratio was underestimated in the afternoon. Since the IN yield applied in the 0D model has +36%/-33% uncertainty, a sensitivity test on the yield was performed. As shown in Figure 8c, the simulated $[IN]/([MVK]+[MACR])$ ratio is highly sensitive to the yield used in the model. The 6% yield significantly underestimated the ratio in the morning, and the 12% yield significantly overestimated the ratio in the afternoon.

4 Discussion

4.1 Model-observation comparison for SOAS data

As shown in Figure 8c, the modeled results deviated from observations from 10:00 AM to 12:00 PM for all the three yields applied. During this period, the simulated $[IN]/([MVK]+[MACR])$ ratio decreased slowly, but the observed ratio dropped rapidly. The fast decrease in the $[IN]/([MVK]+[MACR])$ ratio implies either fast production of MVK+MACR, or fast consumption of IN. In terms of fast production of MVK+MACR, the formation of MVK+MACR from OH and O₃ have been characterized in the model, and the model was capable of simulating MVK+MACR concentration to within measurement uncertainty for the chamber experiments (Supplement 3.1). Therefore, the discrepancy between model and observation is potentially associated with underestimated loss rate of IN. The model results with the 6% yield were lower than observations, despite potential underestimated IN loss rate, so a higher yield (9-12%) may be more accurate to describe the branching ratio for isoprene RO₂+NO reaction.

The model overestimation in the afternoon can be caused collectively by measurement uncertainties for model input, uncertainties in the IN loss rates for OH oxidation and deposition, uncertainties in ambient IN (25%) and MVK+MACR (40%) measurement, and other missing IN loss processes. A recent study found that isoprene hydroperoxide (ISOPOOH) could interfere with MVK and MACR measurement when standard PTR-MS and GC methods are used (Rivera-Rios et al., 2014). We found that the model

appeared to agree better with observations in the afternoon, if the ISOPOOH+IEPOX concentration was subtracted from the MVK+MACR measurement data (Figure 8d). However, the exact influence of ISOPOOH+IEPOX on the observations of MVK+MACR is unclear, as the ISOPOOH conversion efficiency is highly dependent on instrumental sampling configuration, and the interference of IEPOX has not been characterized.

We also considered that an underestimated IN photolysis rate could be one of the reasons for the model-observation discrepancy. The photolysis rate for IN was set to be identical to the photolysis rate for alkyl nitrates in MCMv3.2, but IN isomers have double bonds and hydroxyl groups, which could increase the IN absorption cross section and enhance the photolytic reactivity for IN. When the IN photolysis rate was increased by 5 times for the 9% yield, or 12.5 times for the 12% yield, the simulated $[IN]/([MVK]+[MACR])$ ratio was brought closer to observation in the afternoon, but the IN loss rate still appeared underestimated between 10:00 AM and 12:00 PM (Figure 8e). When the higher photolysis rates were applied, the simulated IN loss to photolysis could contribute up to 30% (9% yield case) or 50% (12% yield case) of total IN loss. Since no experimental data were available on the absorption cross spectrum and quantum yield for IN, large photo-dissociation rate coefficients are purely hypothetical. While photolysis may be a significant IN sink in the ambient environment, its contribution to IN loss in chamber experiments is negligible, as the lamp radiation was ~10% of solar radiation and the durations of the chamber experiments were short. Therefore, no correction for the photolytic loss was made for the IN measurement performed in chamber experiments.

Despite the discrepancy in absolute values, the simulated $[IN]/([MVK]+[MACR])$ ratios all peaked in the morning, consistent with observation. The peak signifies the time when the IN loss rate started to exceed the IN production rate. As the OH-loss lifetime of IN decreased from 8:00 AM to 1:00 PM, the IN production rate (Figure 7b) remained constant during this time. Although isoprene and OH concentrations were both greater after the noontime, the IN production rate did not increase, due to the small γ value. Therefore, the morning IN peak can be attributed to the combined effects of slow IN production and fast IN consumption in the afternoon, with NO_x being the limiting factor for IN production during this field study.

Although the simulated $[IN]/([MVK]+[MACR])$ ratios all peaked in the morning, they peaked one hour later than the observed ratio (Figure 8c). In addition, the modeled ratio had a smaller growth rate than the observed ratio between 7:00 AM and 9:00 AM, regardless of the IN yield and IN loss rate applied (Figure 8c and 8d). This underprediction implies an unknown source of IN, and we can hypothesize that it was caused by downward mixing of the RL IN, as the fast morning increase of IN coincided with inversion breakup. By combining the observations of IN and MVK+MACR during SOAS and the results from the 0D model, we can calculate the growth rate of ambient IN concentration caused solely by isoprene photochemistry in the daytime (Supplement Sect. 7). This photochemical IN growth rate was compared with the observed IN growth rate, and from that we estimate that downward mixing can contribute to $27(\pm 16)\%$ of the fast IN increase in the morning, where the large uncertainty originates from the uncertainty in the IN yield.

The residual layer IN concentration before mixing (6:00 AM) was estimated with the 0D model, using the same initial input as the ground-level observation on the previous day at 8:00 PM. The chemical processes involved are IN production from isoprene oxidation by NO_3 (R5 and R6b) and IN consumption by OH, O_3 and NO_3 . Based on our model calculation, the steady-state NO_3 concentration at night was on the order of 1×10^6 molecules cm^{-3} . Nighttime OH was generated through BVOC ozonolysis, and the simulated concentration was on the order of 5×10^4 molecules cm^{-3} . Even though the OH concentration was very low at night, it was still the dominant IN loss pathway, because of the fast IN+OH reaction rate constants. It is worth noting that RO_2 produced from isoprene + NO_3 (R6) also has competing loss channels for reaction with RO_2 (R7) and with HO_2 (R8). Therefore, only a fraction of the isoprene nitrooxy peroxy radicals (ONO_2RO_2) can react with other peroxy radicals to produce IN through reaction R7b.



Figure 9 shows the simulated IN concentration in the RL and IN observed near ground before dawn, assuming the RL was completely stable at night with no depositional loss for IN from the RL. The simulated IN concentration in the RL before dawn was greater than the concentrations measured at ground level by up to one order of magnitude, indicating the IN stored in the RL overnight may be a significant ground level IN source during inversion breakup. This high IN concentration above the NBL is the result of IN produced during the previous day, which is present with the high concentration in the RL as it is formed, and zero deposition removal overnight. The NO₂ concentration is low when the RL is formed at sunset, so contribution from IN production through NO₃ chemistry is small (1-10ppt), a minor fraction compared with the concentration of IN already present in the RL in the evening. Isoprene-NO₃ chemistry can generate IN isomers with a different isomeric distribution. Since IN production from this reaction scheme is small, no sensitivity correction was performed to account for the changes in isomer distribution when RL IN mixed with ground-level IN in the morning.

The calculated residual layer IN does not take into account the altitude-dependent IN concentration caused by OH oxidation, as well as possible IN concentration change caused by advection. Therefore, the actual IN concentration may be very different from the calculated results. This is reflected in a comparison of the large RL IN excess relative to surface IN on Jun 26 and 27 (Figure 9), with simultaneous model overprediction of daytime IN on these two days (Figure 8a). Hence, detailed three-dimensional chemical transport models are needed to fully elucidate the production and storage mechanisms of IN in the ambient environment.

4.2 High-NO_x and low-NO_x chemistry during SOAS

OH oxidation was the most important daytime sink for BVOCs during SOAS. As the γ value decreased from 0.95 at 7:00 AM to 0.3 at 1:00 PM (Figure 7b), the BVOC-derived RO₂ radicals are expected to undergo both NO (high NO_x) and HO₂ (low NO_x) reaction pathways throughout the day. For isoprene, the presence of the two reaction schemes was signified by the oxidation products, with IN peaking in the morning and ISOPOOH and IEPOX peaking in the afternoon (Figure 10).

As IN was consumed by OH, it would also undertake both NO and HO₂ reaction pathways. Since the highest OH concentrations (1:00 PM) were accompanied with a small γ value (~ 0.3 , Figure 7b), significant amount of IN would be oxidized following the HO₂ pathway. A possible reaction scheme is illustrated in Figure 11 with 1,2-IN as an example.

Experimental studies by Jacobs et al. (2014) suggest that OH addition to IN can invoke IEPOX formation with a yield of 13% at atmospheric pressure, which simultaneously releases NO₂. Although IEPOX can be produced from IN oxidation, the ISOPOOH pathway was still the dominant IEPOX precursor during this study, due to the higher concentrations of ISOPOOH and its higher yield for IEPOX (~ 70 -80%) (St. Clair et al., 2015). For RO₂ radicals produced from OH addition to IN, 30% will react with NO and 70% will react with HO₂ for a γ value of 0.3 at 1:00 PM.

For the RO₂+NO reaction, Lee et al. (2014b) observed the formation of dinitrate for δ isomers of IN and estimated a branching ratio of less than 18% for β -4,3-IN based on missing carbon in the gas phase. The RO radicals from the RO₂+NO reaction will dissociate to make either MACR nitrate or lose NO₂ to form hydroxyacetone and glycoaldehyde. Both Jacobs et al. (2014) and Lee et al. (2014b) reported MACR nitrate being the dominant product with an overall yield of 70%, thus making the corresponding branching ratio for the RO radical to be around 80%.

The RO₂+HO₂ products from IN oxidation are less understood. Alkyl peroxy radical reaction with HO₂ can undergo two reaction channels to afford either hydroperoxide or RO radical and OH. The branching ratio is highly structure dependent. Simple alkyl peroxy radicals, such as CH₃CH₂O₂, can form hydroperoxide with almost unity yield (Hasson et al., 2004). However, for peroxy radicals with β carbonyl groups, such as RC(O)CH₂O₂, the branching ratio for the OH formation pathway is more than 60% (Hasson et al., 2012; Hasson et al., 2004). The β carbonyl oxygen can stabilize the reaction intermediate through internal hydrogen bonding, thus making the reaction favor the formation of OH and RO (Hasson et al., 2005). The RO₂ from IN oxidation has a β -OH group and a β -NO₃ group, both capable of forming internal hydrogen bonding with the hydrogen of HO₂. Therefore, formation of OH and RO radicals may be a significant

reaction channel when the RO₂ radicals derived from IN react with HO₂. The closed-shell product from the RO₂+HO₂ reaction is dihydroxy hydroperoxy nitrate (DHHPN). This compound has not been identified in any laboratory studies. However, Lee et al. (2015) found a significant amount of compounds with the corresponding molecular formula of C₅H₁₁O₇N in the aerosol phase during SOAS, which suggests that hydroperoxide formation and aerosol uptake could be an important sink for IN.

A range can be estimated for the NO₂ recycling efficiency for IN oxidation, as the detailed RO₂+HO₂ reaction mechanism is unclear. If RO₂+HO₂ reaction forms only hydroperoxide, the NO₂ yield from IN oxidation will be 17%. If RO₂+HO₂ reaction only undergoes the radical formation channel, the NO₂ yield will be 30%, and the major products of IN oxidation are highly oxidized secondary nitrates.

5 Summary and atmospheric implications

Our chamber experiments indicate a 9(+4/-3)% nitrate yield from isoprene hydroxyperoxy radical reaction with NO. The product yield provides a more reliable groundwork for future modeling studies on the interplay of isoprene oxidation, NO_x cycling, and tropospheric O₃ production.

Our field measurements and model simulations suggest that in the southeast US, formation of organic nitrates in the boundary layer is controlled by the availability of NO_x. During the SOAS field study, when isoprene was oxidized by OH addition, the NO peak in the morning on average consumed 95% of the isoprene RO₂ to form high NO_x photooxidation products such as IN, MVK and MACR. As the NO_x concentration decreased during the day, the RO₂+HO₂ reactions became more important, and by ~1:00 PM only 30% of the RO₂ react with NO, and thus only 2.7% of the RO₂ would form organic nitrates. The high NO_x concentration in the early morning caused an early IN maximum at 10:00 AM, a combined result of slow afternoon IN production with limited NO_x, and fast IN consumption due to peak radiation and fast OH production in the afternoon. By comparing simulation results with observations, we estimate the inversion breakup after sunrise may contribute to 27(±16)% of the rapid IN increase in the morning. The observed daytime IN loss can be approximated with the current understanding of IN oxidation reactions and dry deposition, but some discrepancies still

exist, which could be caused by other less studied loss pathways, such as nitrate photolysis. Aerosol uptake could also be an IN sink, but the contribution is expected to be small (Surratt et al., 2010b). Observations during SOAS suggest that the isoprene-derived SOA components were associated with IEPOX and more oxidized organic nitrates, not the first-generation hydroxynitrates (Xu et al., 2015b; Lee et al., 2015).

While IN were produced and destroyed in the morning through high NO_x chemistry, a major portion of the afternoon IN oxidation process involved low NO_x chemistry, which could yield products such as the highly oxidized dihydroxy hydroperoxy nitrate (DHHPN). DHHPN is expected to have very low vapor pressure and undergo fast dry deposition and aerosol partitioning, possibly followed by hydrolysis and formation of NO_3^- and trihydroxy hydroperoxide. This process removes NO_x from the atmosphere and helps to shift the photochemical processes further toward the low NO_x regime, forming a positive feedback mechanism to reduce the atmospheric NO_x concentration. However, more experimental studies are required to elucidate the detailed mechanism for the $\text{RO}_2 + \text{HO}_2$ reactions.

During the past 15 years, NO_x emissions in the southeastern US have decreased by more than 50% (Hidy et al., 2014). As more effort is devoted to controlling anthropogenic emissions, the BVOC oxidation processes will start to shift further toward the low NO_x regime. Isoprene products resulting from oxidation in the low NO_x condition, such as IEPOX, are more prone to reactive uptake and thus contribute more effectively to the growth of SOA than IN (Xu et al., 2015a; Surratt et al., 2010a; Nguyen et al., 2014a), indicating potentially higher SOA burdens from isoprene chemistry in the future. The low NO_x photochemistry is often complicated by radical reactions including intramolecular H-shift and autoxidation (So et al., 2014; Peeters et al., 2014; Savee et al., 2015; Crounse et al., 2013), so more theoretical and experimental studies of the fundamental reaction kinetics are needed to unravel the complete BVOC oxidation mechanism. The photochemical reactions that involve both the high NO_x and low NO_x pathways can yield new highly-oxidized multi-functional nitrate products. Identification, quantification and study of the chemistry of these organic nitrates is essential to understand the fate of NO_x . As the highly-oxidized compounds, such as DHHPN and dintrate, tend to partition into

the aerosol phase, it will be a challenge for the development of analytical techniques to investigate their aging process in the particle phase and their role in the NO_x cycle.

Acknowledgement

We thank the organizers of the SOAS study, especially Dr. Ann Marie Carlton. We appreciate help from Dr. Jozef Peeters at University of Leuven in elucidating the uncertainties associated with the current LIM1 mechanism. We acknowledge funding from the National Science Foundation (NSF) grant 1228496 and US Environmental Protection Agency (EPA) STAR grant 83540901.

References

- Atkinson, R., Aschmann, S. M., Carter, W. P. L., Winer, A. M., and Pitts, J. N.: Alkyl nitrate formation from the nitrogen oxide (NO_x)-air photooxidations of C₂-C₈ n-alkanes, *The Journal of Physical Chemistry*, 86, 4563-4569, 10.1021/j100220a022, 1982.
- Bates, K. H., Crounse, J. D., St Clair, J. M., Bennett, N. B., Nguyen, T. B., Seinfeld, J. H., Stoltz, B. M., and Wennberg, P. O.: Gas phase production and loss of isoprene epoxydiols, *The journal of physical chemistry. A*, 118, 1237-1246, 10.1021/jp4107958, 2014.
- Beaver, M. R., St Clair, J. M., Paulot, F., Spencer, K. M., Crounse, J. D., LaFranchi, B. W., Min, K. E., Pusede, S. E., Wooldridge, P. J., Schade, G. W., Park, C., Cohen, R. C., and Wennberg, P. O.: Importance of biogenic precursors to the budget of organic nitrates: observations of multifunctional organic nitrates by CIMS and TD-LIF during BEARPEX 2009, *Atmospheric Chemistry and Physics*, 12, 5773-5785, 10.5194/acp-12-5773-2012, 2012.
- Carter, W. P. L., and Atkinson, R.: Development and evaluation of a detailed mechanism for the atmospheric reactions of isoprene and NO_x, *International Journal of Chemical Kinetics*, 28, 497-530, 10.1002/(SICI)1097-4601(1996)28:7<497::AID-KIN4>3.0.CO;2-Q, 1996.
- Chen, X., Hulbert, D., and Shepson, P. B.: Measurement of the organic nitrate yield from OH reaction with isoprene, *Journal of Geophysical Research*, 103, 25563, 10.1029/98jd01483, 1998.
- Crounse, J. D., McKinney, K. A., Kwan, A. J., and Wennberg, P. O.: Measurement of Gas-Phase Hydroperoxides by Chemical Ionization Mass Spectrometry, *Analytical chemistry*, 78, 6726-6732, 10.1021/ac0604235, 2006.
- Crounse, J. D., Paulot, F., Kjaergaard, H. G., and Wennberg, P. O.: Peroxy radical isomerization in the oxidation of isoprene, *Physical chemistry chemical physics : PCCP*, 13, 13607-13613, 10.1039/c1cp21330j, 2011.
- Crounse, J. D., Nielsen, L. B., Jørgensen, S., Kjaergaard, H. G., and Wennberg, P. O.: Autoxidation of Organic Compounds in the Atmosphere, *The Journal of Physical Chemistry Letters*, 4, 3513-3520, 10.1021/jz4019207, 2013.
- Day, D. A., Wooldridge, P. J., Dillon, M. B., Thornton, J. A., and Cohen, R. C.: A thermal dissociation laser-induced fluorescence instrument for in situ detection of NO₂, peroxy nitrates, alkyl nitrates, and HNO₃, *Journal of Geophysical Research: Atmospheres*, 107, ACH 4-1-ACH 4-14, 10.1029/2001JD000779, 2002.

712 Fan, J., and Zhang, R.: Atmospheric Oxidation Mechanism of Isoprene, *Environmental Chemistry*,
 713 1, 140, 10.1071/en04045, 2004.

714 Giacomelli, P., Ford, K., Espada, C., and Shepson, P. B.: Comparison of the measured and
 715 simulated isoprene nitrate distributions above a forest canopy, *Journal of Geophysical Research*,
 716 110, D01304, 10.1029/2004jd005123, 2005.

717 Gilman, J. B., Burkhardt, J. F., Lerner, B. M., Williams, E. J., Kuster, W. C., Goldan, P. D., Murphy, P.
 718 C., Warneke, C., Fowler, C., Montzka, S. A., Miller, B. R., Miller, L., Oltmans, S. J., Ryerson, T. B.,
 719 Cooper, O. R., Stohl, A., and de Gouw, J. A.: Ozone variability and halogen oxidation within the
 720 Arctic and sub-Arctic springtime boundary layer, *Atmos. Chem. Phys.*, 10, 10223-10236,
 721 10.5194/acp-10-10223-2010, 2010.

722 Grosjean, D., Williams, E. L., and Grosjean, E.: Atmospheric chemistry of isoprene and of its
 723 carbonyl products, *Environmental science & technology*, 27, 830-840, 10.1021/es00042a004,
 724 1993.

725 Grossenbacher, J. W., Couch, T., Shepson, P. B., Thornberry, T., Witmer-Rich, M., Carroll, M. A.,
 726 Faloona, I., Tan, D., Brune, W., Ostling, K., and Bertman, S.: Measurements of isoprene nitrates
 727 above a forest canopy, *Journal of Geophysical Research*, 106, 24429, 10.1029/2001jd900029,
 728 2001.

729 Grossenbacher, J. W., Barket Jr, D. J., Shepson, P. B., Carroll, M. A., Olszyna, K., and Apel, E.: A
 730 comparison of isoprene nitrate concentrations at two forest-impacted sites, *Journal of*
 731 *Geophysical Research: Atmospheres*, 109, D11311, 10.1029/2003JD003966, 2004.

732 Guenther, A., Karl, T., Harley, P., Wiedinmyer, C., Palmer, P. I., and Geron, C.: Estimates of global
 733 terrestrial isoprene emissions using MEGAN (Model of Emissions of Gases and Aerosols from
 734 Nature), *Atmos. Chem. Phys.*, 6, 3181-3210, 10.5194/acp-6-3181-2006, 2006.

735 Hao, C., Shepson, P. B., Drummond, J. W., and Muthuramu, K.: Gas Chromatographic Detector
 736 for Selective and Sensitive Detection of Atmospheric Organic Nitrates, *Analytical chemistry*, 66,
 737 3737-3743, 10.1021/ac00093a032, 1994.

738 Hartsell, B. E., Aneja, V. P., and Lonneman, W. A.: Relationships between peroxyacetyl nitrate,
 739 O₃, and NO_y at the rural Southern Oxidants Study site in central Piedmont, North Carolina, site
 740 SONIA, *Journal of Geophysical Research: Atmospheres*, 99, 21033-21041, 10.1029/94JD01021,
 741 1994.

742 Harwood, L. M., Casy, G., and Sherlock, J.: A Simple Laboratory Procedure for Preparation of (1-
 743 Methylethenyl)oxirane (3,4-Epoxyisoprene), *Synthetic Communications*, 20, 1287-1292,
 744 10.1080/00397919008052839, 1990.

745 Hasson, A. S., Tyndall, G. S., and Orlando, J. J.: A Product Yield Study of the Reaction of HO₂
 746 Radicals with Ethyl Peroxy (C₂H₅O₂), Acetyl Peroxy (CH₃C(O)O₂), and Acetonyl Peroxy
 747 (CH₃C(O)CH₂O₂) Radicals, *The Journal of Physical Chemistry A*, 108, 5979-5989,
 748 10.1021/jp048873t, 2004.

749 Hasson, A. S., Kuwata, K. T., Arroyo, M. C., and Petersen, E. B.: Theoretical studies of the
 750 reaction of hydroperoxy radicals (HO₂) with ethyl peroxy (CH₃CH₂O₂), acetyl peroxy
 751 (CH₃C(O)O₂), and acetonyl peroxy (CH₃C(O)CH₂O₂) radicals, *Journal of Photochemistry and*
 752 *Photobiology A: Chemistry*, 176, 218-230, <http://dx.doi.org/10.1016/j.jphotochem.2005.08.012>,
 753 2005.

754 Hasson, A. S., Tyndall, G. S., Orlando, J. J., Singh, S., Hernandez, S. Q., Campbell, S., and Ibarra, Y.:
 755 Branching ratios for the reaction of selected carbonyl-containing peroxy radicals with
 756 hydroperoxy radicals, *The journal of physical chemistry. A*, 116, 6264-6281, 10.1021/jp211799c,
 757 2012.

758 Hastie, D. R., Shepson, P. B., Sharma, S., and Schiff, H. I.: The influence of the nocturnal
 759 boundary layer on secondary trace species in the atmosphere at Dorset, Ontario, *Atmospheric*
 760 *Environment. Part A. General Topics*, 27, 533-541, [http://dx.doi.org/10.1016/0960-](http://dx.doi.org/10.1016/0960-1686(93)90210-P)
 761 [1686\(93\)90210-P](http://dx.doi.org/10.1016/0960-1686(93)90210-P), 1993.

762 Hidy, G. M., Blanchard, C. L., Baumann, K., Edgerton, E., Tanenbaum, S., Shaw, S., Knipping, E.,
 763 Tombach, I., Jansen, J., and Walters, J.: Chemical climatology of the southeastern United States,
 764 1999–2013, *Atmospheric Chemistry and Physics*, 14, 11893-11914, 10.5194/acp-14-
 765 11893-2014, 2014.

766 Horowitz, L. W., Fiore, A. M., Milly, G. P., Cohen, R. C., Perring, A., Wooldridge, P. J., Hess, P. G.,
 767 Emmons, L. K., and Lamarque, J.-F.: Observational constraints on the chemistry of isoprene
 768 nitrates over the eastern United States, *Journal of Geophysical Research*, 112, D12S08,
 769 10.1029/2006jd007747, 2007.

770 Hu, K. S., Darer, A. I., and Elrod, M. J.: Thermodynamics and kinetics of the hydrolysis of
 771 atmospherically relevant organonitrates and organosulfates, *Atmospheric Chemistry and*
 772 *Physics*, 11, 8307-8320, 10.5194/acp-11-8307-2011, 2011.

773 Jacobs, M. I., Burke, W. J., and Elrod, M. J.: Kinetics of the reactions of isoprene-derived
 774 hydroxynitrates: gas phase epoxide formation and solution phase hydrolysis, *Atmospheric*
 775 *Chemistry and Physics*, 14, 8933-8946, 10.5194/acp-14-8933-2014, 2014.

776 Jenkin, M. E., Saunders, S. M., and Pilling, M. J.: The tropospheric degradation of volatile organic
 777 compounds: a protocol for mechanism development, *Atmospheric Environment*, 31, 81-104,
 778 [http://dx.doi.org/10.1016/S1352-2310\(96\)00105-7](http://dx.doi.org/10.1016/S1352-2310(96)00105-7), 1997.

779 Kwan, A. J., Chan, A. W. H., Ng, N. L., Kjaergaard, H. G., Seinfeld, J. H., and Wennberg, P. O.:
 780 Peroxy radical chemistry and OH radical production during the NO₃-initiated
 781 oxidation of isoprene, *Atmospheric Chemistry and Physics*, 12, 7499-7515, 10.5194/acp-12-
 782 7499-2012, 2012.

783 Lee, B. H., Lopez-Hilfiker, F. D., Mohr, C., Kurtén, T., Worsnop, D. R., and Thornton, J. A.: An
 784 Iodide-Adduct High-Resolution Time-of-Flight Chemical-Ionization Mass Spectrometer:
 785 Application to Atmospheric Inorganic and Organic Compounds, *Environmental science &*
 786 *technology*, 48, 6309-6317, 10.1021/es500362a, 2014a.

787 Lee, B. H., Mohr, C., Lopez-Hilfiker, F. D., D'Ambro1, E. L., Lutz, A., Hallquist, M., Lee, L., Romer,
 788 P., Cohen, R. C., Iyer, S., Kurten, T., Hu, W. W., Day, D. A., Campuzano-Jost, P., Jimenez, J. L., Xu,
 789 L., Ng, N. L., Wild, R. J., Brown, S. S., Koss, A., Gouw, J. d., Olson, K., Goldstein, A. H., Seco, R.,
 790 Kim, S., McAvey, K., Shepson, P. B., Baumann, K., Edgerton, E. S., Nguyen, T. B., Wennberg, P. O.,
 791 Liu, J., Shilling, J. E., and Thornton, J. A.: Highly functionalized particle-phase organic nitrates
 792 observed in the Southeastern U.S.: contribution to secondary organic aerosol and reactive
 793 nitrogen budgets, in preparation, 2015.

794 Lee, L., Teng, A. P., Wennberg, P. O., Crounse, J. D., and Cohen, R. C.: On rates and mechanisms
 795 of OH and O₃ reactions with isoprene-derived hydroxy nitrates, *The journal of physical*
 796 *chemistry. A*, 118, 1622-1637, 10.1021/jp4107603, 2014b.

797 Liao, J., Sihler, H., Huey, L. G., Neuman, J. A., Tanner, D. J., Friess, U., Platt, U., Flocke, F. M.,
 798 Orlando, J. J., Shepson, P. B., Beine, H. J., Weinheimer, A. J., Sjostedt, S. J., Nowak, J. B., Knapp,
 799 D. J., Staebler, R. M., Zheng, W., Sander, R., Hall, S. R., and Ullmann, K.: A comparison of Arctic
 800 BrO measurements by chemical ionization mass spectrometry and long path-differential optical
 801 absorption spectroscopy, *Journal of Geophysical Research*, 116, D00R02,
 802 10.1029/2010jd014788, 2011.

803 Liu, Y. J., Herdinger-Blatt, I., McKinney, K. A., and Martin, S. T.: Production of methyl vinyl
 804 ketone and methacrolein via the hydroperoxyl pathway of isoprene oxidation, *Atmospheric
 805 Chemistry and Physics*, 13, 5715-5730, 10.5194/acp-13-5715-2013, 2013.

806 Lockwood, A. L., Shepson, P. B., Fiddler, M. N., and Alaghmand, M.: Isoprene nitrates:
 807 preparation, separation, identification, yields, and atmospheric chemistry, *Atmospheric
 808 Chemistry and Physics*, 10, 6169-6178, 10.5194/acp-10-6169-2010, 2010.

809 Madronich, S., and Flocke, S.: The role of solar radiation in atmospheric chemistry, in: *Handbook
 810 of Environmental Chemistry*, edited by: Boule, P., Springer-Verlag, Heidelberg, 1-26, 1998.

811 Mielke, L. H., Pratt, K. A., Shepson, P. B., McLuckey, S. A., Wisthaler, A., and Hansel, A.:
 812 Quantitative Determination of Biogenic Volatile Organic Compounds in the Atmosphere Using
 813 Proton-Transfer Reaction Linear Ion Trap Mass Spectrometry, *Analytical chemistry*, 82, 7952-
 814 7957, 10.1021/ac1014244, 2010.

815 Misztal, P. K., Guenther, A., and Goldstein, A. H.: Flux observations of isoprene oxidation
 816 products above forests point to potential role of leaf-surface reactions, In preparation.

817 Neu, U., Künzle, T., and Wanner, H.: On the relation between ozone storage in the residual layer
 818 and daily variation in near-surface ozone concentration — A case study, *Boundary-Layer
 819 Meteorol*, 69, 221-247, 10.1007/BF00708857, 1994.

820 Nguyen, T. B., Coggon, M. M., Bates, K. H., Zhang, X., Schwantes, R. H., Schilling, K. A., Loza, C. L.,
 821 Flagan, R. C., Wennberg, P. O., and Seinfeld, J. H.: Organic aerosol formation from the reactive
 822 uptake of isoprene epoxydiols (IEPOX) onto non-acidified inorganic seeds, *Atmospheric
 823 Chemistry and Physics*, 14, 3497-3510, 10.5194/acp-14-3497-2014, 2014a.

824 Nguyen, T. B., Crounse, J. D., Schwantes, R. H., Teng, A. P., Bates, K. H., Zhang, X., St. Clair, J. M.,
 825 Brune, W. H., Tyndall, G. S., Keutsch, F. N., Seinfeld, J. H., and Wennberg, P. O.: Overview of the
 826 Focused Isoprene eXperiment at the California Institute of Technology (FIXCIT): mechanistic
 827 chamber studies on the oxidation of biogenic compounds, *Atmospheric Chemistry and Physics*,
 828 14, 13531-13549, 10.5194/acp-14-13531-2014, 2014b.

829 Nguyen, T. B., Crounse, J. D., Teng, A. P., St Clair, J. M., Paulot, F., Wolfe, G. M., and Wennberg,
 830 P. O.: Rapid deposition of oxidized biogenic compounds to a temperate forest, *Proceedings of
 831 the National Academy of Sciences of the United States of America*, 10.1073/pnas.1418702112,
 832 2015.

833 O'Brien, J. M., Shepson, P. B., Muthuramu, K., Hao, C., Niki, H., Hastie, D. R., Taylor, R., and
 834 Roussel, P. B.: Measurements of alkyl and multifunctional organic nitrates at a rural site in
 835 Ontario, *Journal of Geophysical Research: Atmospheres*, 100, 22795-22804,
 836 10.1029/94JD03247, 1995.

837 Patchen, A. K., Pennino, M. J., Kiep, A. C., and Elrod, M. J.: Direct kinetics study of the product-
 838 forming channels of the reaction of isoprene-derived hydroxyperoxy radicals with NO,
 839 *International Journal of Chemical Kinetics*, 39, 353-361, 10.1002/kin.20248, 2007.

840 Paulot, F., Crounse, J. D., Kjaergaard, H. G., Kroll, J. H., Seinfeld, J. H., and Wennberg, P. O.:
 841 Isoprene photooxidation: new insights into the production of acids and organic nitrates, *Atmos.*
 842 *Chem. Phys.*, 9, 1479-1501, 10.5194/acp-9-1479-2009, 2009.

843 Paulot, F., Henze, D. K., and Wennberg, P. O.: Impact of the isoprene photochemical cascade on
 844 tropical ozone, *Atmospheric Chemistry and Physics*, 12, 1307-1325, 10.5194/acp-12-1307-2012,
 845 2012.

846 Peeters, J., Nguyen, T. L., and Vereecken, L.: HOx radical regeneration in the oxidation of
 847 isoprene, *Physical chemistry chemical physics : PCCP*, 11, 5935-5939, 10.1039/b908511d, 2009.

848 Peeters, J., Müller, J.-F., Stavrou, T., and Nguyen, V. S.: Hydroxyl Radical Recycling in Isoprene
 849 Oxidation Driven by Hydrogen Bonding and Hydrogen Tunneling: The Upgraded LIM1
 850 Mechanism, *The Journal of Physical Chemistry A*, 118, 8625-8643, 10.1021/jp5033146, 2014.

851 Perring, A. E., Wisthaler, A., Graus, M., Wooldridge, P. J., Lockwood, A. L., Mielke, L. H., Shepson,
 852 P. B., Hansel, A., and Cohen, R. C.: A product study of the isoprene+NO₃ reaction, *Atmos. Chem.*
 853 *Phys.*, 9, 4945-4956, 10.5194/acp-9-4945-2009, 2009.

854 Rindelaub, J. D., McAvey, K. M., and Shepson, P. B.: The photochemical production of organic
 855 nitrates from α -pinene and loss via acid-dependent particle phase hydrolysis, *Atmospheric*
 856 *Environment*, 100, 193-201, <http://dx.doi.org/10.1016/j.atmosenv.2014.11.010>, 2015.

857 Rivera-Rios, J. C., Nguyen, T. B., Crounse, J. D., Jud, W., St. Clair, J. M., Mikoviny, T., Gilman, J. B.,
 858 Lerner, B. M., Kaiser, J. B., de Gouw, J., Wisthaler, A., Hansel, A., Wennberg, P. O., Seinfeld, J. H.,
 859 and Keutsch, F. N.: Conversion of hydroperoxides to carbonyls in field and laboratory
 860 instrumentation: Observational bias in diagnosing pristine versus anthropogenically controlled
 861 atmospheric chemistry, *Geophysical Research Letters*, n/a-n/a, 10.1002/2014gl061919, 2014.

862 Rollins, A. W., Kiendler-Scharr, A., Fry, J. L., Brauers, T., Brown, S. S., Dorn, H. P., Dubé, W. P.,
 863 Fuchs, H., Mensah, A., Mentel, T. F., Rohrer, F., Tillmann, R., Wegener, R., Wooldridge, P. J., and
 864 Cohen, R. C.: Isoprene oxidation by nitrate radical: alkyl nitrate and secondary organic aerosol
 865 yields, *Atmos. Chem. Phys.*, 9, 6685-6703, 10.5194/acp-9-6685-2009, 2009.

866 Rollins, A. W., Smith, J. D., Wilson, K. R., and Cohen, R. C.: Real Time In Situ Detection of Organic
 867 Nitrates in Atmospheric Aerosols, *Environmental science & technology*, 44, 5540-5545,
 868 10.1021/es100926x, 2010.

869 Saunders, S. M., Jenkin, M. E., Derwent, R. G., and Pilling, M. J.: Protocol for the development of
 870 the Master Chemical Mechanism, MCM v3 (Part A): tropospheric degradation of non-aromatic
 871 volatile organic compounds, *Atmos. Chem. Phys.*, 3, 161-180, 10.5194/acp-3-161-2003, 2003.

872 Savee, J. D., Papajak, E., Rotavera, B., Huang, H., Eskola, A. J., Welz, O., Sheps, L., Taatjes, C. A.,
 873 Zádor, J., and Osborn, D. L.: Direct observation and kinetics of a hydroperoxyalkyl radical
 874 (QOOH), *Science*, 347, 643-646, 10.1126/science.aaa1495, 2015.

875 Schwantes, R. H., Teng, A. P., Nguyen, T. B., Coggon, M. M., Crounse, J. D., St. Clair, J. M., Zhang,
 876 X., Schilling, K. A., Seinfeld, J. H., and Wennberg, P. O.: Isoprene NO₃ Oxidation Products from
 877 the RO₂ + HO₂ Pathway, *The Journal of Physical Chemistry A*, 10.1021/acs.jpca.5b06355, 2015.

878 So, S., Kirk, B. B., Trevitt, A. J., Wille, U., Blanksby, S. J., and da Silva, G.: Unimolecular reaction
 879 chemistry of a charge-tagged beta-hydroxyperoxyl radical, *Physical Chemistry Chemical Physics*,
 880 16, 24954-24964, 10.1039/C4CP02981J, 2014.

881 Sprengnether, M., Demerjian, K. L., Donahue, N. M., and Anderson, J. G.: Product analysis of the
 882 OH oxidation of isoprene and 1,3-butadiene in the presence of NO, *Journal of Geophysical*
 883 *Research*, 107, 10.1029/2001jd000716, 2002.

884 St. Clair, J. M., Rivera, J. C., Crounse, J. D., Knap, H. C., Bates, K. H., Teng, A. P., Jørgensen, S.,
 885 Kjaergaard, H. G., Keutsch, F. N., and Wennberg, P. O.: Kinetics and Products of the Reaction of
 886 the First-Generation Isoprene Hydroxy Hydroperoxide (ISOPOOH) with OH, *The Journal of*
 887 *Physical Chemistry A*, 10.1021/acs.jpca.5b06532, 2015.

888 Stevens, P., L'Esperance, D., Chuong, B., and Martin, G.: Measurements of the kinetics of the
 889 OH-initiated oxidation of isoprene: Radical propagation in the OH + isoprene + O₂ + NO reaction
 890 system, *International Journal of Chemical Kinetics*, 31, 637-643, 10.1002/(SICI)1097-
 891 4601(1999)31:9<637::AID-KIN5>3.0.CO;2-O, 1999.

892 Stutz, J.: Vertical profiles of NO₃, N₂O₅, O₃, and NO_x in the nocturnal boundary layer: 1.
 893 Observations during the Texas Air Quality Study 2000, *Journal of Geophysical Research*, 109,
 894 D12306, 10.1029/2003jd004209, 2004.

895 Surratt, J. D., Chan, A. W., Eddingsaas, N. C., Chan, M., Loza, C. L., Kwan, A. J., Hersey, S. P.,
 896 Flagan, R. C., Wennberg, P. O., and Seinfeld, J. H.: Reactive intermediates revealed in secondary
 897 organic aerosol formation from isoprene, *Proceedings of the National Academy of Sciences of*
 898 *the United States of America*, 107, 6640-6645, 10.1073/pnas.0911114107, 2010a.

899 Surratt, J. D., Chan, A. W. H., Eddingsaas, N. C., Chan, M., Loza, C. L., Kwan, A. J., Hersey, S. P.,
 900 Flagan, R. C., Wennberg, P. O., and Seinfeld, J. H.: Reactive intermediates revealed in secondary
 901 organic aerosol formation from isoprene, *Proceedings of the National Academy of Sciences of*
 902 *the United States of America*, 107, 6640-6645, 10.1073/pnas.0911114107, 2010b.

903 Teng, A. P., Crounse, J. D., Lee, L., St. Clair, J. M., Cohen, R. C., and Wennberg, P. O.: Hydroxy
 904 nitrate production in the OH-initiated oxidation of alkenes, *Atmos. Chem. Phys.*, 15, 4297-4316,
 905 10.5194/acp-15-4297-2015, 2015.

906 Tuazon, E. C., and Atkinson, R.: A product study of the gas-phase reaction of Isoprene with the
 907 OH radical in the presence of NO_x, *International Journal of Chemical Kinetics*, 22, 1221-1236,
 908 10.1002/kin.550221202, 1990.

909 Xie, Y., Paulot, F., Carter, W. P. L., Nolte, C. G., Luecken, D. J., Hutzell, W. T., Wennberg, P. O.,
 910 Cohen, R. C., and Pinder, R. W.: Understanding the impact of recent advances in isoprene
 911 photooxidation on simulations of regional air quality, *Atmospheric Chemistry and Physics*, 13,
 912 8439-8455, 10.5194/acp-13-8439-2013, 2013.

913 Xu, L., Guo, H., Boyd, C. M., Klein, M., Bougiatioti, A., Cerully, K. M., Hite, J. R., Isaacman-
 914 VanWertz, G., Kreisberg, N. M., Knute, C., Olson, K., Koss, A., Goldstein, A. H., Hering, S. V., de
 915 Gouw, J., Baumann, K., Lee, S. H., Nenes, A., Weber, R. J., and Ng, N. L.: Effects of anthropogenic
 916 emissions on aerosol formation from isoprene and monoterpenes in the southeastern United
 917 States, *Proceedings of the National Academy of Sciences of the United States of America*, 112,
 918 37-42, 10.1073/pnas.1417609112, 2015a.

919 Xu, L., Suresh, S., Guo, H., Weber, R. J., and Ng, N. L.: Aerosol characterization over the
 920 southeastern United States using high-resolution aerosol mass spectrometry: spatial and
 921 seasonal variation of aerosol composition and sources with a focus on organic nitrates,
 922 *Atmospheric Chemistry and Physics*, 15, 7307-7336, 10.5194/acp-15-7307-2015, 2015b.

Zhang, L., Moran, M. D., Makar, P. A., Brook, J. R., and Gong, S.: Modelling gaseous dry deposition in AURAMS: a unified regional air-quality modelling system, Atmospheric Environment, 36, 537-560, [http://dx.doi.org/10.1016/S1352-2310\(01\)00447-2](http://dx.doi.org/10.1016/S1352-2310(01)00447-2), 2002.

Zhao, J., and Zhang, R.: A theoretical investigation of nitrooxyalkyl peroxy radicals from NO₃-initiated oxidation of isoprene, Atmospheric Environment, 42, 5849-5858, <http://dx.doi.org/10.1016/j.atmosenv.2007.09.023>, 2008.

Table 1. Hydroxynitrates from OH-initiated isoprene oxidation (high NO_x).

β-INs				
	1,2-IN	2,1-IN	3,4-IN	4,3-IN
δ-INs				
	<i>cis</i> -1,4-IN	<i>trans</i> -1,4-IN	<i>cis</i> -4,1-IN	<i>trans</i> -4,1-IN

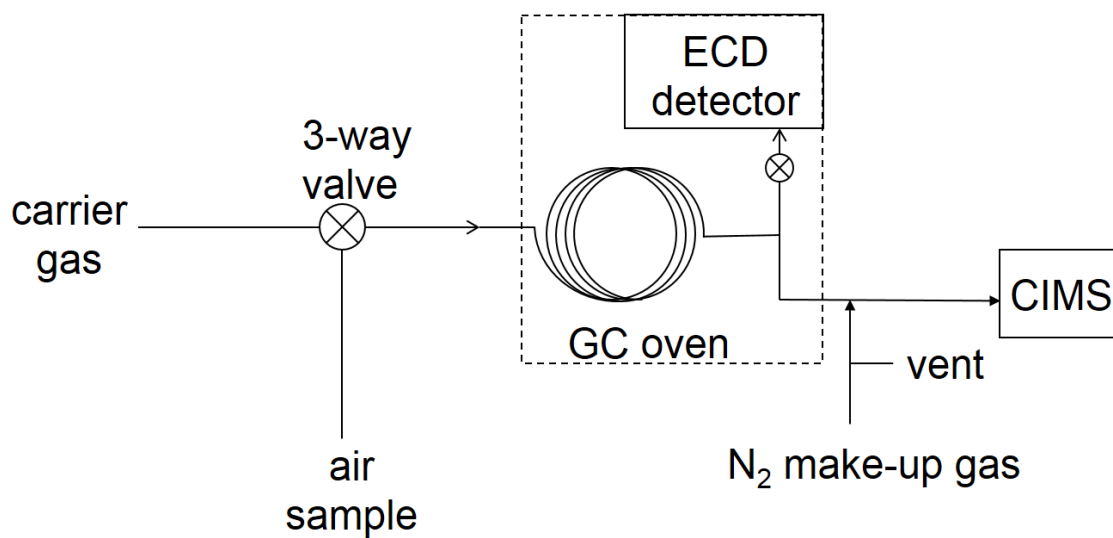
Table 2. Initial conditions for IN yield experiments.

Expt. number	Isoprene (ppb)	Isopropyl nitrite (ppb)	NO (ppb)	Expt. duration (min)
-----------------	-------------------	-------------------------------	-------------	----------------------------

1	140	180	160	16
2	80	180	130	15
3	70	180	130	12
4	120	180	125	14
5	90	180	220	14
6	75	180	210	12
7	85	180	2400	54

939

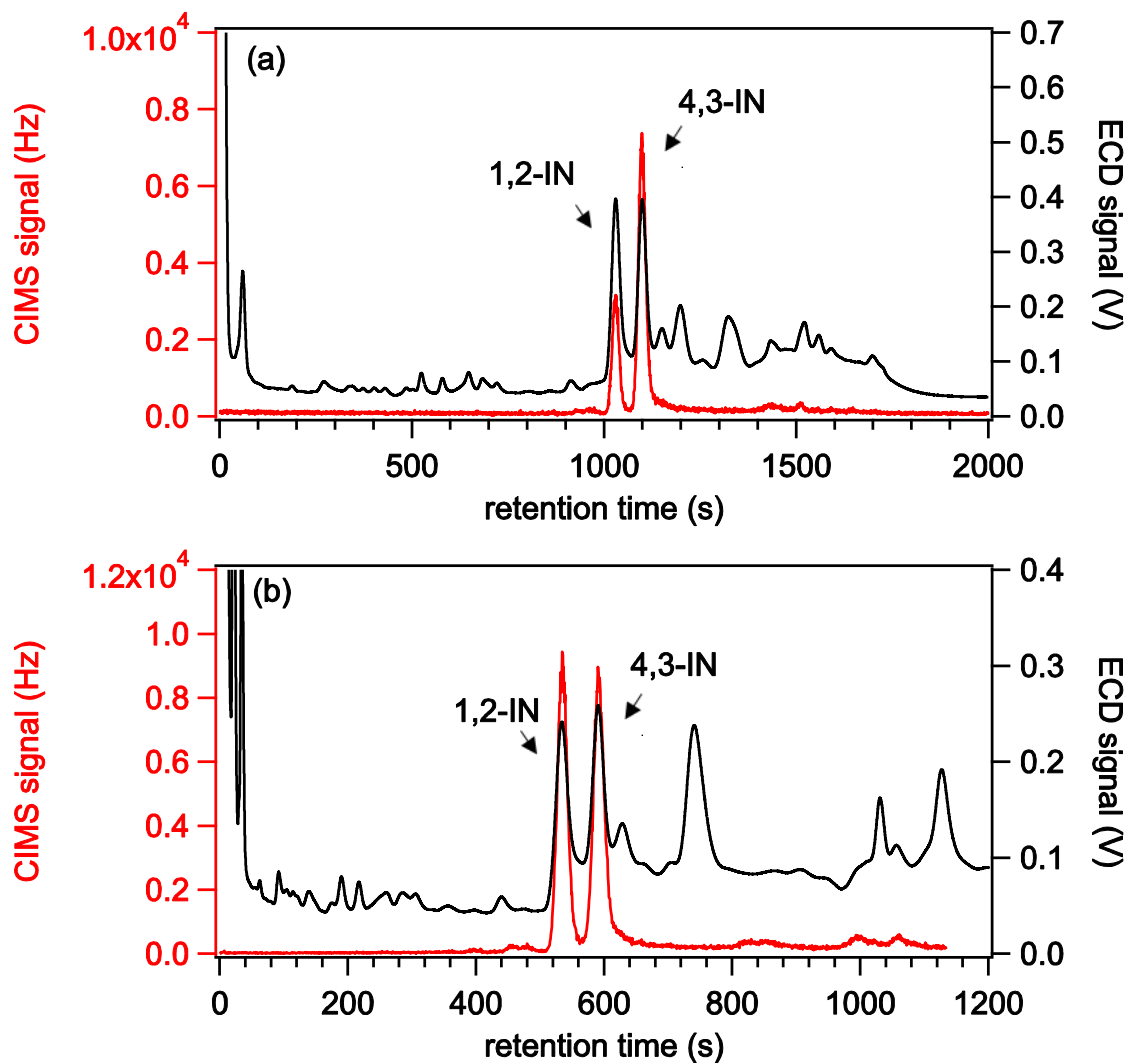
940



941

942 Figure 1. GC-ECD/CIMS setup for the CIMS sensitivity of 1,2-IN relative to 4,3-IN.

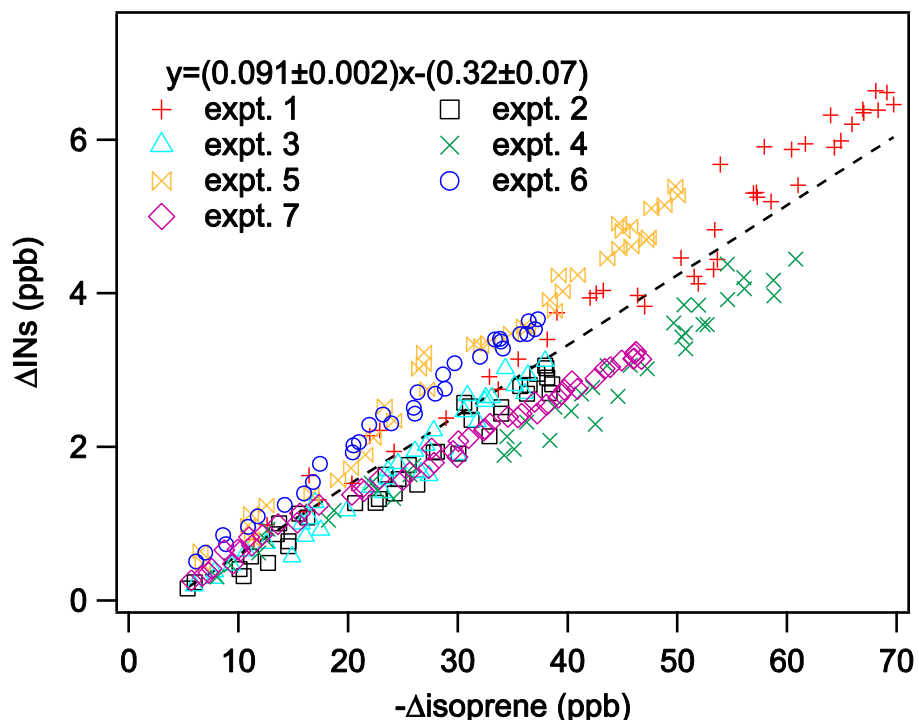
943



944

945 Figure 2. GC-ECD/CIMS chromatogram with water (a) and without water (b) added to
 946 the CIMS. The ECD signal is in black and the CIMS signal is in red.

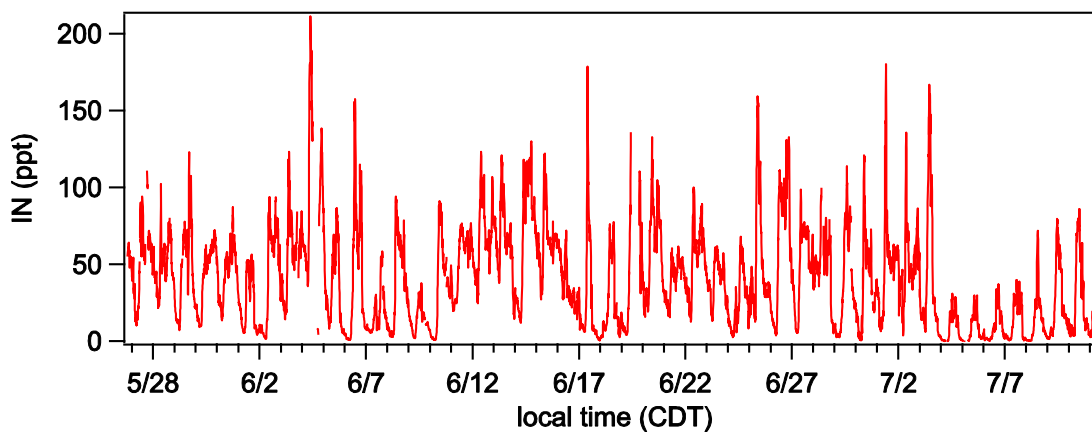
947



948

949 Figure 3. IN and isoprene data for chamber experiments. An average yield of 9% was
 950 obtained from data of the seven experiments.

951



952

953 Figure 4. IN observed during SOAS.

954

955

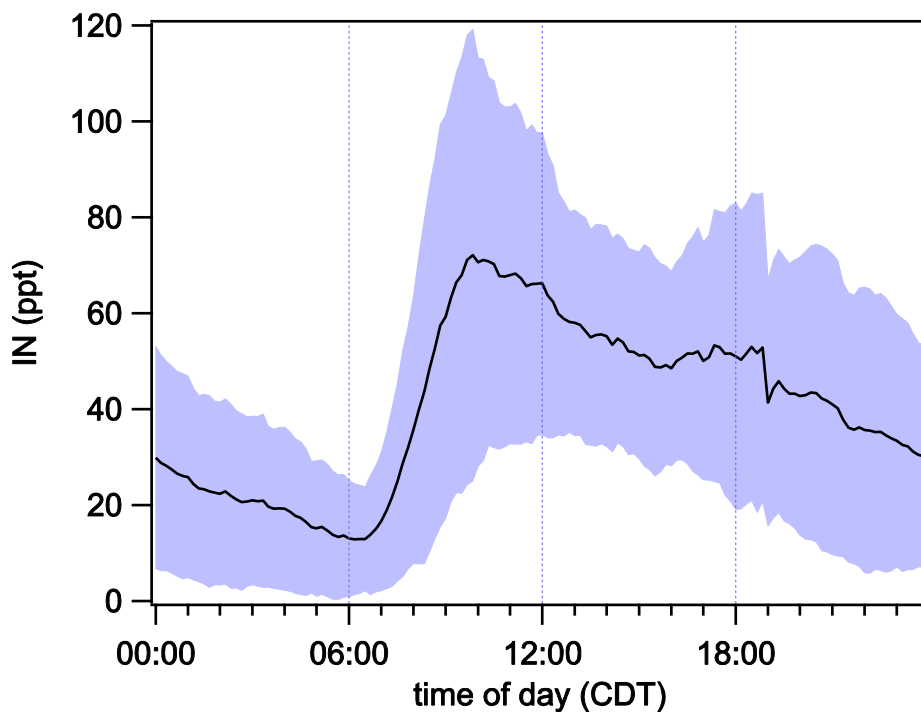


Figure 5. IN diurnal average from May 28 to Jul 11. The blue shade indicates day-to-day variation (1σ). The abrupt drop of concentration at 7 PM is caused by instrument fluctuation during its daily maintenance.

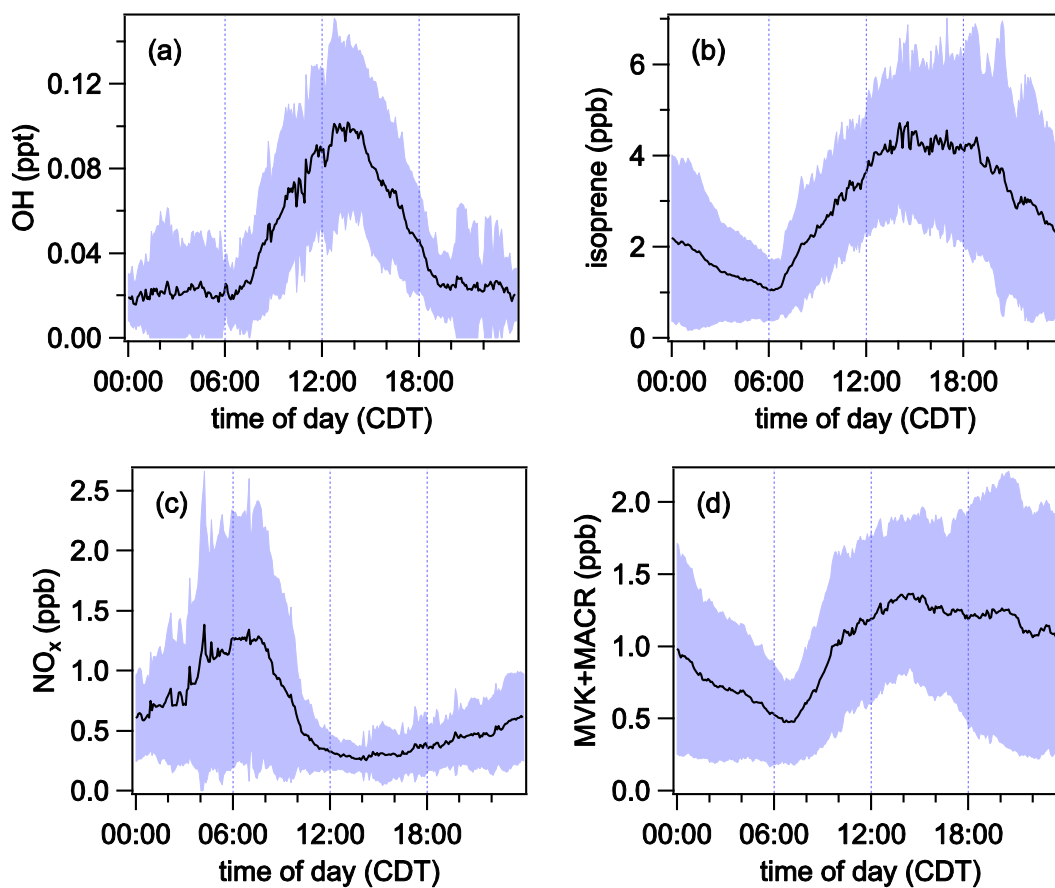


Figure 6. Diurnal average of OH (a, Jun 13 - Jul 3), isoprene (b, Jun 16 - Jul 11), NO_x (c, Jun 1 - Jul 15) and sum of MVK and MACR (d, Jun 16 - Jul 11).

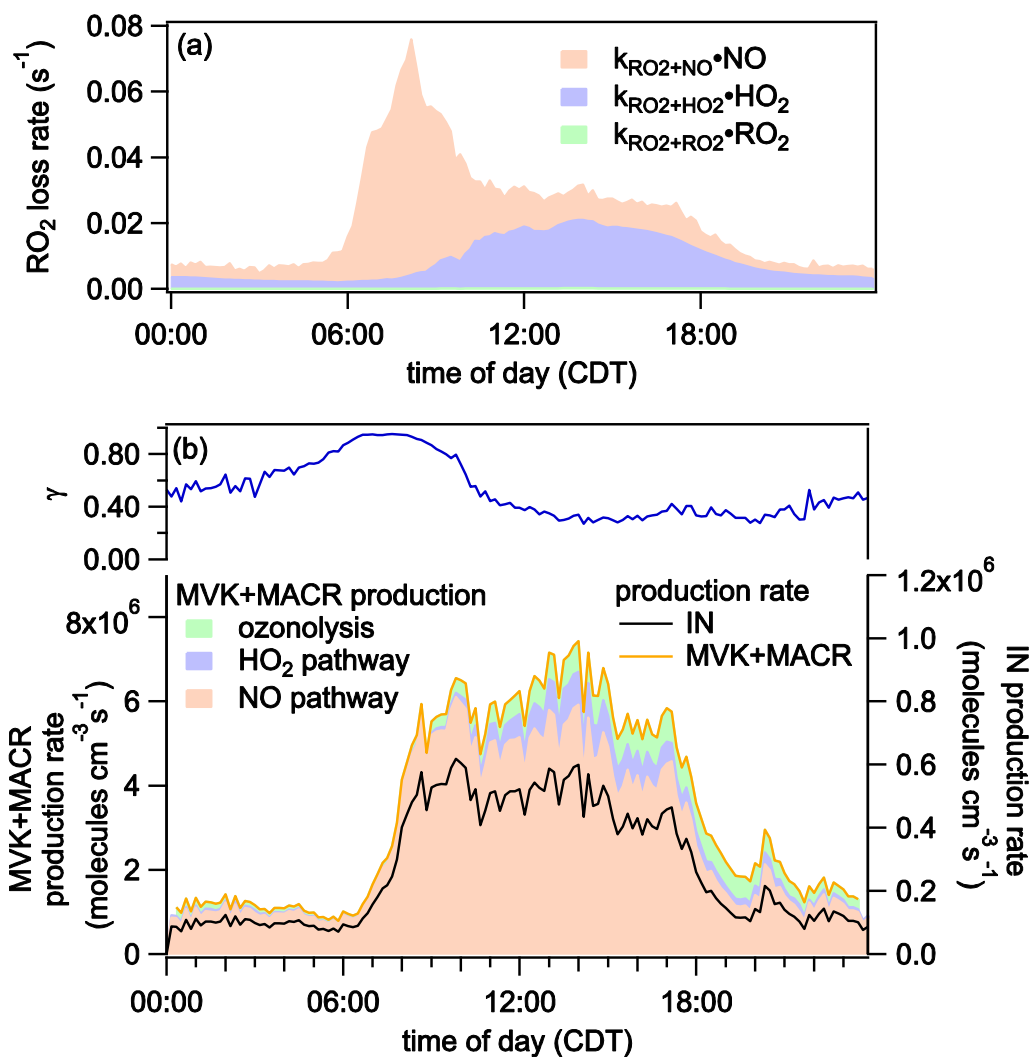


Figure 7. (a) Diurnal average of RO₂ loss rates for reaction with NO, HO₂ and RO₂ from Jun 22 to Jul 7. (b) Diurnal average of γ value and production rates of IN and MVK+MACR from Jun 22 to Jul 7. For MVK+MACR, production from the three reaction channels are shown in different colors.

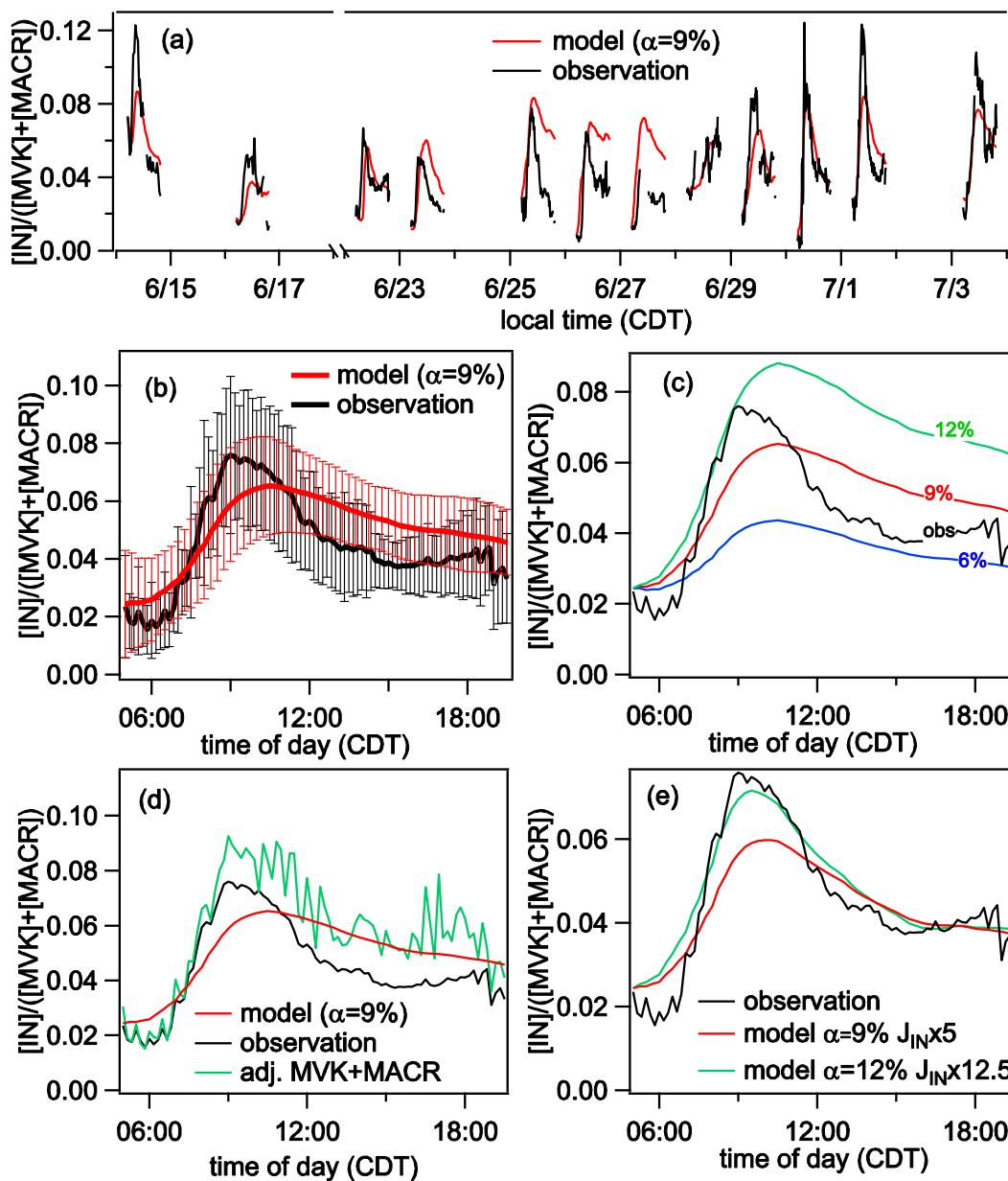
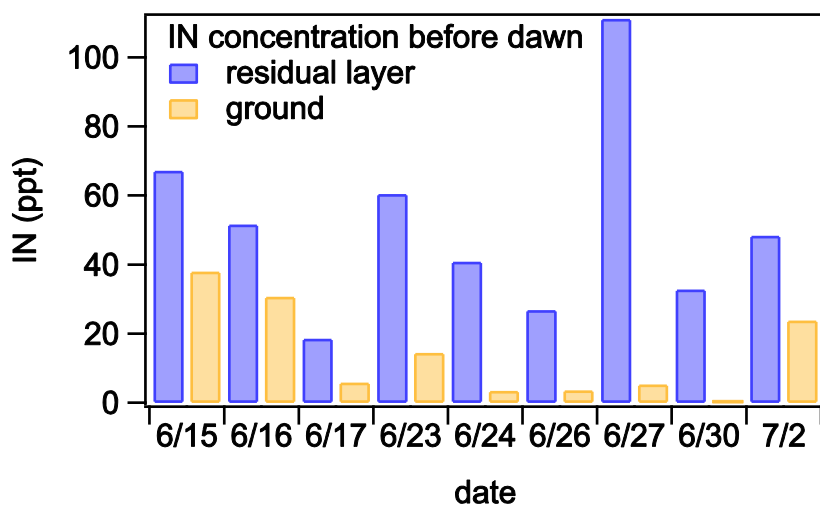


Figure 8. Simulated and observed $[IN]/([MVK]+[MACR])$ ratio. (a) Results for each selected days. (b) Averaged results over the 12 days. The error bars represent day-to-day variation. (c) Sensitivity test with IN yield set as 6%, 9% and 12% in the model. (d) MVK+MACR data was adjusted by subtracting observed IEPOX+ISOPOOH concentration from observed MVK+MACR concentration. (e) Results with enhanced IN photolysis rate.

979



980

981

982 Figure 9 Modeled IN in the residual layer and IN observed near ground before dawn the
 983 next day. The model includes IN production from isoprene oxidation by NO_3 and IN
 984 consumption by reaction with OH, O_3 and NO_3 . The modeled IN may be biased, as
 985 concentration change caused by transport is not considered.

986

